



## Modelling of hollow core concrete construction exposed to fire

David Lange and Robert Jansson McNamee



**Brandforsk**

## KEYWORDS

prestressed concrete, hollow core slabs, fire, modelling

**BRANDFORSK 2016:6**  
**ISBN 978-91-88349-54-5**



## Abstract

This report summarises the results of a project which was intended to study the response of hollow core and prestressed concrete construction exposed to fire. Two fires in the past 12 years highlighted the susceptibility of this type of construction to fire, a car park fire in Rotterdam and a department store fire in Vantaa. The car park fire has been extensively studied elsewhere and has led to much research on the response of hollow core construction exposed to fire. The department store fire has been less well reported.

The report gives a short overview of these two fires, and then reports on a literature review of the response of prestressed and hollow core concrete construction exposed to fire. The comprehensive analyses carried out elsewhere are an excellent starting point for further study.

The report then goes on to discuss the application of different concrete models to prestressed concrete construction. Other work reported elsewhere shows that results of modelling prestressed concrete construction exposed to fire is very susceptible to the concrete model which is used, and so finite element modelling of two fire tests of hollow core slabs is carried out to evaluate the impact of the concrete model on this type of construction. It is found that an explicit formulation of transient strain in concrete has a significant impact compared with an implicit formulation of transient strain, in the overall behaviour of the hollow core slab and also in the response of, e.g. the prestressing tendons.

Finally, an analytical method for assessing the capacity of prestressed concrete construction under ambient conditions is extended to apply to hollow core slabs exposed to fire. This is used to compare the response of prestressed hollow core slabs to prestressed monolithic slabs exposed to fire and to study different parameters which influence the response and the capacity of hollow core units in fire.

Based on the results of the analytical modelling, it can be seen that hollow core concrete construction experiences a far higher thermal gradient and resulting thermal moment than monolithic concrete construction. This is a result of the geometry of the cross section which effectively traps heat in the lower flange. This in turn leads to a faster loss of prestressing force on the cross section than in a monolithic concrete section. This contributes to a faster reduction in the ultimate moment of hollow core slabs compared with monolithic concrete construction.

However changing the prestressing tendon depth has a significant effect on the evolution of the ultimate moment under fire exposure. A shallow tendon with little cover has higher capacity at ambient and under fire exposure for a short duration, whereas a tendon with a large amount of cover has a lower ambient capacity, but retains more of this capacity for longer under fire exposure.

The analytical method which is proposed is not capable of capturing the nuances in behaviour and response of the finite element method which is reported, nevertheless it is useful in helping to understand the response of prestressed concrete construction exposed to fire. It may also be useful as a screening tool for evaluating the impact of different design options either in hollow core slabs themselves or when making choices in the design phase. However, both the analytical and the numerical modelling suffer from a lack of good quality experimental data which could be used for their evaluation and this should be considered in the future.

**Key words:** prestressed concrete, hollow core slabs, fire, modelling

**SP Sveriges Tekniska Forskningsinstitut**  
SP Technical Research Institute of Sweden

SP Report 2016:52  
ISBN 978-91-88349-54-5  
ISSN 0284-5172  
Borås 2016

# Contents

<b>Nomenclature</b>	<b>6</b>
<b>1 Introduction</b>	<b>8</b>
1.1 Background	8
1.1.1 Gretzenbach	9
1.1.2 Rotterdam	10
1.1.3 Vantaa	11
1.1.4 Design of prestressed concrete construction in fire	12
1.2 Outline	13
1.3 Limitations	13
<b>2 Modelling of prestressed concrete construction</b>	<b>14</b>
2.1 Introduction	14
2.2 Transient strain or Load Induced Thermal Strain	14
2.3 Application of transient strain model	17
2.3.1 Test details	17
2.3.2 Numerical modelling	19
2.3.2.1 Heat transfer analysis	20
2.3.2.2 Mechanical analysis	21
2.4 Results	24
2.4.1 SP18 Slab	24
2.4.2 SP22 Slab	25
2.5 Discussion	28
<b>3 Analytical modelling of prestressed concrete construction</b>	<b>30</b>
3.1 Introduction	30
3.2 Methodology	30
3.3 Heat transfer analysis	31
3.4 Thermo-mechanical response of the cross section	31
3.5 Calculation of temperature dependent prestressing force	37
3.6 Calculation of thermally induced displacements	39
3.7 Load bearing capacity	42
<b>4 Influencing the ultimate moment of prestressed concrete construction</b>	<b>46</b>
4.1 Cover to reinforcement	46
4.2 Prestressing force	49
4.3 Section geometry	51
<b>5 Discussion and conclusions</b>	<b>53</b>
<b>6 References</b>	<b>55</b>

## Nomenclature

In general an effort has been made to make the nomenclature clear throughout the text, however all of the variables used in the equations throughout this report are described briefly here for reference.

Latin letters:

$A$	Area
$A_i$	Area of slice $i$
$A_{ps}$	Area of prestressing steel
$b$	Breadth of concrete section
$E$	Modulus of elasticity
$E_i$	Modulus of elasticity of slice $i$
$E_{ref}$	Reference modulus of elasticity
$E_{pre,T}$	Temperature dependent modulus of elasticity of prestressing tendons
$E_{pre,\infty}$	Ambient temperature modulus of elasticity of prestressing tendons
$F_{cc}$	Compressive force in concrete
$f_{cu}$	Compressive strength of concrete
$F_i$	Thermally induced force in a slice $i$
$F_T$	Thermally induced force in a section
$F_{tot}$	Total force in the cross section from thermal effects and prestressing load
$F_{pre,T}$	Prestressing force at temperature $T$
$F_{pre,\infty}$	Ambient temperature prestressing force
$F_{ts}$	Tensile force in steel
$I$	Second moment of area
$I_i$	Second moment of area of slice $i$
$k_1, k_2$	Factors describing the shape of the concrete stress block
$L$	Length
$m_i$	Modular ratio of slice $i$
$M_{tot}$	Total moment in the cross section from thermal effects and prestressing load
$M_{pre,T}$	Temperature dependent moment from the prestressing tendons
$M_T$	Thermally induced moment in a section
$T$	Temperature
$\Delta T$	Temperature increase
$\Delta T_c$	Temperature increase of concrete
$\Delta T_i$	Temperature increase of slice $i$
$\Delta T_s$	Temperature increase of steel
$t$	Time
$u$	End displacement
$w_T$	Thermally induced displacement
$w_{pre,T}$	Total thermally induced displacement accounting for prestressing effects
$y_c$	Depth to the centroid of the modified concrete section
$y_{pre}$	Depth to the level of the prestressing tendons
$z_i$	Depth of slice $i$ from a reference position, $\bar{z}$

Greek letters:

$\alpha_c$	Coefficient of thermal expansion of concrete
$\alpha_i$	Coefficient of thermal expansion of a slice $i$
$\alpha_s$	Coefficient of thermal expansion of steel

$\varepsilon$	Strain
$\varepsilon_c$	Compressive strain in concrete from prestressing load
$\varepsilon_{cr}$	Creep strain
$\varepsilon_{cu}$	Ultimate strain of concrete
$\varepsilon_{pa}$	Total strain in concrete at the level of the prestressing tendon, at the ultimate moment of a loaded section
$\varepsilon_{pb,T}$	Tendon strain at the ultimate moment of a loaded section
$\varepsilon_{pre,T}$	Strain in prestressing steel at temperature T
$\varepsilon_T$	Thermal strain in prestressing steel
$\varepsilon_{th}$	Thermal strain
$\varepsilon_{tot}$	Equivalent contraction strain
$\varepsilon_{tr}$	Transient strain
$\varepsilon_u$	Mechanical strain in prestressing steel at the ultimate moment of a loaded section
$\varepsilon_\sigma$	Mechanical strain
$\Phi_{pre,T}$	Curvature induced by the prestressing tendons at increased temperature
$\Phi_T$	Thermally induced curvature
$\Phi_{tot,T}$	Total curvature from the prestressing tendons and the thermal curvature
$\sigma$	Stress
$\tilde{\sigma}$	Stress history
$\sigma_{pb}$	Stress in prestressing tendons
$\omega_{tot}$	Total end rotation

# 1 Introduction

## 1.1 Background

Over the last 20 years, structural fire engineering has developed rapidly based on a dramatic increase in the knowledge of the response of structures to fire. In part this has been fuelled by incidents in real buildings such as the Broadgate fire and the World Trade Centre tower collapses; or planned testing programmes, such as the Cardington tests. But overall it has been made possible by advances in computing power which have allowed engineers to better understand the impact of fires on structures.

Most of the research to date has focussed on the behaviour of composite steel / concrete structures or on reinforced concrete structures, and significant advances have been made in these areas. However, failures as a result of fire in other types of construction highlight the need for additional work to be done which focuses on different construction types, specifically prestressed hollow core concrete construction. Fire induced failures of precast hollow core slabs highlight a disparity between the expected and the actual performance in fire of these types of construction [1].

Traditional structural design for fire is based upon the response of a structural element to a standard fire, usually this response is determined by a furnace test. A single element is subjected to a standard fire for some prescribed duration during which the capacity of the element is checked to ensure that it meets relevant requirements in terms of displacement and rate of displacement under constant loading. Testing therefore focuses on the loss of stiffness and strength of the material and the element, and where the component fails by passing a stated displacement limit or rate of displacement, passive fire protection can be applied to ensure that the component does not reach the critical temperature needed to pass that limit for the duration of the furnace test.

Because of the low conductivity and high density of concrete, and the fact that a certain amount of concrete is needed for carrying the load in the cold state, concrete is typically seen to be more naturally fire resistant than steel – it is effectively self-insulating – and so design of steel structures has focussed on protection of the elements so that they may meet the requirements of the fire resistance test in the same way, and a lot of research has been done to optimise this. While this has resulted in an improved understanding of the response of steel to fire, there remains much which can be done to improve the understanding of concrete structures response to fire. Some research has been done in the past to understand the principles of the behaviour of concrete structures in fire, especially in Sweden, both regarding material properties in fire [2], and modelling of behaviour during parametric fire exposure [3]. In 1988, Pettersson published a review of the requirements for structural fire design highlighting, for example, the requirements for a testing regime to better understand concrete as a material in fire [4]. In 1991, Anderberg and Pettersson published their “Fire Resistance Dimensioning Of Concrete Constructions” in Swedish [5], which contained a summary of much of their research to date and included recommendations for detailing of reinforced concrete structures for fire resistance. Little work had been done on understanding steel structures up to this point and, as noted above, the focus was largely on protection since it was generally regarded that deformation and loss of stiffness and strength of steel in fire would lead to structural failure.

However, in 1990, a fire broke out in the partially completed structure of Broadgate phase 8 in London – a 14 storey steel composite office building which was largely completed but which had no passive fire protection installed. The building did not collapse, although it did suffer very large deflections as a result of the elevated temperatures [6]. This was

contrary to popular understanding of fire resistance and although it was widely known at the time that failure of elements in a real fire inside of a highly redundant structure bears little resemblance to failure of elements in a furnace test [7], the Broadgate fire led to a more focussed and concerted effort to understand real frame behaviour in real fires. This was made manifest in the Cardington tests – 6 full scale fire tests carried out on a composite steel / concrete structure undertaken jointly by British Steel and the Building Research Establishment (BRE) – following which a consortium undertook to analyse the results and to aid in the understanding of the underlying mechanics which govern structural response to fire [8].

Results of this work quickly led to a characterisation of the membrane mechanism in composite slabs, and to the development of design tools [9, 10, 11] which are now frequently used in practice.

More recently than Broadgate, the Linköping public library fire occurred in 1996 within a two storey reinforced concrete frame [12]. The fire started on the second floor. The building was subject to significant damage which occurred after only 30 minutes of fire exposure despite having been designed with 60 minutes fire resistance in mind. Conclusions from the investigation highlighted architectural features as a contributing factor to the intensity of the fire, and the restraint against expansion of the very long span floor which led to shear failure at the walls as a contributing factor to the structural failure, Figure 1.1. Ultimately restraint effects and compatibility rotations in the surrounding structure were highlighted as important considerations for design.

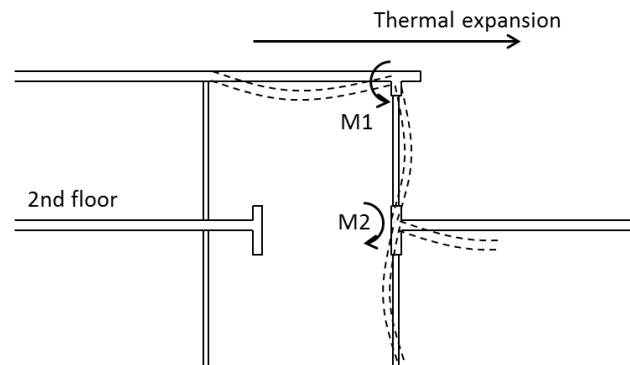


**Figure 1.1 – failure mechanism in the Linköping public library, redrawn from [12]**

Modern concrete construction, however, makes use of many different technologies compared with traditional reinforced concrete structures. Several events over the last few years have highlighted the lack of understanding of the behaviour of other types of concrete construction in fire – and highlight the need for more research to better understand the behaviour of these construction types.

For example, recent events have included: the car park fire in Gretzenbach, Switzerland in 2004; a multi-storey car park fire in Rotterdam in 2007; and the Hong Kong department store fire in Vantaa, Finland around Christmas 2010. Each of these events will be discussed in more detail below.

### 1.1.1 Gretzenbach

In Gretzenbach, Switzerland, in 2004, a fire occurred in an underground car park. The structure was made of reinforced concrete, and while fighting the fire, 7 firefighters were killed when the structural slab collapsed on top of them. Failure in this instance has been

attributed to punching shear at the columns [13]. Studies of this event have resulted in proposals for increasing the shear resistance of floor slabs at columns by means of post-installed bonded shear reinforcement bars [14]. Further work on punching shear failure has led to further guidance for ambient temperature design [15]. However no additional guidance for fire resistance is known to have arisen as a result of this for inclusion as a natural part of the initial design process.

Nevertheless, work to understand this mechanism is still ongoing. Recent publications include a comparison of an analytical design formulation, extended with the temperature dependent material properties from the Eurocode, with experiments [16]; as well as an experimental and a numerical study of the effect of eccentric loading on punching shear failure of concrete slabs in fire [17].

### **1.1.2 Rotterdam**

In Lloyd Street in Rotterdam a fire broke out in a multi storey car park located beneath an apartment complex in 2007. Shortly after the start of the fire, the bodies of the hollow core slabs, of which the structure was comprised, split horizontally and the lower half fell to the floor below [1, 18]. Although not a complete collapse of the floor slab, this type of failure had never been seen before and led to much work in the Netherlands studying the effect of fire on hollow core slabs. Some of this work was published in a special issue of Cement in 2011 and further results of this were summarised in an open letter from the BFBN in the Netherlands in November 2009 and then in an updated letter in June 2011 [19] including the following conclusions:

- If the restraint provided by a thick layer or topcoat is sufficient to restrict deformation, horizontal cracks in the webs of the hollow-core slab occur as a result of which the lower flanges of the slabs can fail. This is a consequence of the behaviour in the transverse direction of the hollow-core slab that is dominant with respect to the behaviour in the longitudinal direction.
- It is expected that in a top layer thickness of up to and including 50 mm there will be no issues with the lower part of the slab. Above 70 mm there is evidence that horizontal formation of cracks in the webs and then loosening of the lower flange may occur.
- As a result of the loss due to fire of the lower flange, the reduction in self weight means that in some cases the top layer in the hollow core slab will still meet the requirements of building regulations.
- For hollow core floors it is necessary to distinguish between the collapse of the lower flange, the local collapse of the floor field, and the situation where disproportionate damage in accordance with the Eurocodes to the entire structure occurs.



**Figure 1.2 – damage to the hollow core slabs in Rotterdam following a fire in a car park [20]**

### 1.1.3 Vantaa

On the 24<sup>th</sup> of December 2010 at around 4 o'clock in the afternoon a fire broke out in the warehouse of the Hong Kong department store in Vantaa, Finland [21, 22]. The building was concrete framed with a hollow core slab deck and was constructed in 1986. In the space above the fire seat, cracks were found by fire fighters along with deformation of the floor surface. The cracks allowed the transfer of smoke between the room of origin and the floor above. Response crews reported a strong jolt within the building approximately 1 hr after ignition and were given the order to evacuate. Approximately 10 to 15 minutes after this, failure of the first hollow-core slab was observed and fire spread upstairs. The first collapse was followed by several more collapses of the hollow core slabs [23]. The building had been designed for 2 hours fire resistance. Luckily no one was killed.



**Figure 1.3 – damage to the hollow core slabs in Vantaa, Finland; left shows delamination of the lower flange, right shows the void left following collapse of one of the floors [23]**

The official report into the fire [23] highlighted the geometry of the compartment as well as the restraint provided to the floor slabs as having contributed to their early collapse. The significant heating to the underside of the slabs caused rapid heating which in turn induced in-plane thermal expansion at the bottom of the floor. This expansion was restrained by the monolithic structure surrounding the floor slabs which experienced little damage or deflection.

### 1.1.4 Design of prestressed concrete construction in fire

In comparison with massive concrete floors, a hollow core floor requires 30 % less concrete and 50 % less steel [24]. HC units are normally 1.2 m wide, 0.2 to 0.4 m thick and can be up to 20 m long. In-situ grouted longitudinal joints and longitudinal and transverse ties connect the units to each other and facilitate load distribution in the transverse direction. HC units provide good flexural capacity over long spans due to longitudinal prestressed strands. They are therefore a popular construction option for buildings such as industrial buildings, offices, apartments and parking garages.

Some research has been done to study the response of hollow core slabs in fire. These have included experimental and analytical / numerical studies. In Perugia in Italy, a test program was undertaken to study the response of loaded HC floor slabs in fire, [25]. The tests performed comprised a standard furnace test without restraint at the slabs perimeter but were loaded to 60% of the service load. A summary of recent tests is included in [26], along with details of numerical work which was undertaken. No parametric study was undertaken except for an investigation of free, pinned or restrained translation at the boundaries.

Shear and anchorage failures have been highlighted as potential failure mechanisms which should be considered in design along with the support conditions [27]. In instances where the anchorage between the tendon in hollow core slabs fails locally; a local relaxation of prestressing may cause cracking of the concrete and tension stiffening of the steel reinforcement may spread the cracked region propagating this failure mode.

Some work has been done to investigate the impact of fires on unbonded post tensioned floor slabs [28, 29], where the relaxation of prestress as a result of thermal expansion of the steel is highlighted as an issue.

Fellinger conducted a significant review of fire testing on HC slabs [30]. He reviewed criteria including strand temperature, moisture and load level and their statistical impact upon failure in fire tests. In his work, Fellinger also conducted additional tests, in some cases loaded around the perimeter. Additional material testing focussed on pull-out of the prestressing tendon. Ultimately his work focussed on studying a failure in shear, induced by loss of anchorage of the tendon as a result of bond slippage under high temperature. This was further supported by numerical work which considered the transfer of the prestressing force. Fellinger concluded that shear anchorage failure must be considered during the design of HC units.

According to the European Organisation for Technical Approvals (EOTA) [31], the fire performance of prefabricated building units and concrete frame building kits may be demonstrated by following relevant Structural Eurocodes. The performance of the HC slab system may therefore be demonstrated by means of either fire testing, simple calculation methods or advanced calculation methods [32]. However, the fire resistance which is obtained from standard testing on these elements does not necessarily account for the support conditions and connection detailing, which could play a significant role in the behaviour and response of these elements [33]. Further, the spans which are typically achieved using these elements are larger than what is physically possible to test in the majority of furnaces available.

In addition to this, the simple calculation methods are based on a reduced cross-section, ignoring the contribution of concrete over a given temperature to the overall strength or based on a strength reduction of the material caused by the increased temperature. In any

event, the simple calculations do not explicitly require thermal expansion of concrete or steel to be considered.

## 1.2 Outline

The scope of this project has been focussed around contributing to an evolving understanding of the behaviour of prestressed concrete construction, and hollow core construction in particular.

In carrying out the work the initial intention was to rely on numerical tools, specifically the finite element method, to evaluate the interaction between these types of construction and the supporting structure. However difficulties in applying numerical tools and benchmarking these based on existing test reports led the focus to shift during the project to extending and developing analytical tools and methods. These are used to evaluate the response of prestressed concrete construction to fire in order to demonstrate the impact of various design choices on the response of prestressed construction.

There are three distinct sections in this study:

- The first describes numerical modelling of prestressed hollow core concrete slabs; with reference in particular to the concrete material model which is suitable for modelling of prestressed concrete construction and comparison of models to one set of experiments which are reported in the literature.
- The second section describes the extension of an analytical tool for evaluating the response of concrete slabs exposed to fire to prestressed hollow core slabs and compares their response with monolithic concrete slabs of the same thickness. This analytical tool allows for the deformation and the ultimate moment of prestressed and hollow core concrete construction to be calculated, taking account of the loss of prestress as a result of thermal expansion of the prestressing tendons.
- In the third part of the report a discussion through example is given of the impact of various factors on the response of hollow core and prestressed construction to fire; including the overall deflections and the ultimate moment of the sections.

Finally, recommendations for directions for future research which is needed are made based on the results in other parts of this study.

## 1.3 Limitations

One of the issues which structural fire engineering faces is one of validation. Where existing test reports are available then numerical and or analytical models may be validated based on these. However it was difficult to find suitable validation cases for the work which is reported herein. The tests which were initially chosen were later found to be of limited value because of concerns with the experimental setup, and the short duration of the fire exposure, and while the analytical methods presented are extensions of existing methods for the design of prestressed concrete construction at ambient conditions based on relatively simple sectional analyses they have not been validated in application to high temperature.

This is a major limitation of the work which has been undertaken, and it is recommended that future studies of prestressed concrete construction in fire bear this in mind and that a suitable experimental programme is designed to accompany any analytical or numerical work for the purposes of validation.

## 2 Modelling of prestressed concrete construction

### 2.1 Introduction

For advanced calculation methods, Eurocode 2 describes the total strain in concrete in terms of the sum of 4 components [32], the thermal strain,  $\varepsilon_{th}$ ; the instantaneous stress-dependent strain,  $\varepsilon_{\sigma}$ ; the creep strain,  $\varepsilon_{cr}$ ; and the transient state, or transient, strain,  $\varepsilon_{tr}$ :

$$\varepsilon = \varepsilon_{th}(T) + \varepsilon_{\sigma}(\sigma, T) + \varepsilon_{cr}(\sigma, T, t) + \varepsilon_{tr}(\sigma, T) \quad (2.1)$$

Where the thermal strain is dependent upon the temperature  $T$ ; the mechanical strain is dependent upon the current stress state,  $\sigma$ , and the temperature; the creep strain is dependent upon the stress, temperature and time,  $t$ ; and the transient strain which is dependent upon the stress and the temperature (no dependence on time is included in this component). It is also acknowledged that the stress related strain is also dependent upon the stress history,  $\tilde{\sigma}$ , e.g. [34]. Therefore the stress-dependent strain term may in fact be written  $\varepsilon_{\sigma}(\sigma, \tilde{\sigma}, T)$ . Because of the time scale required for creep strains to develop, these are often omitted from structural fire calculations. This reduces the total strain as defined above to be a function of the free thermal expansion strains, the stress induced strains and the transient strain.

### 2.2 Transient strain or Load Induced Thermal Strain

Transient strain, or transient thermal strain, and load induced thermal strain (LITS) are terms which are often used interchangeably. They describe variously a number of components depending upon the definition used by the author, including, e.g. basic creep strain, transient creep, and shrinkage. Law presented a review of the mechanisms which contribute to LITS in his thesis [35]. His definition of LITS was: "LITS is the difference between the free thermal expansion of concrete and the thermal expansion when the same concrete is heated under a level of pre-stress". This is in general agreement with Anderberg and Thelandersson's definition of transient strain which is 'that part of the total strain obtained in stressed concrete under heating that cannot be accounted for otherwise [2], i.e. from the other components of the total strain in concrete discussed above. On the other hand, LITS as defined by Khoury also includes the basic creep, as well as the temperature induced change in elastic strain and a transient creep term which may also be easily confused with the term transient strain [34].

These two definitions are illustrated in Figure 2.1. This section of the report is concerned with a discussion of the impact of transient strain on the response of heated concrete structures.

In the Eurocode, specifically EN1992-1-2:2004 [32], transient strain is not explicitly dealt with and its apparent local relaxing effects are accounted for in heated concrete implicitly. That is to say that to include the effect from transient strain the strain parameters required to define the stress-strain curve at high temperature are artificially increased beyond their 'actual' values. This is done by increasing the crushing strain of concrete, thereby decreasing the tangent modulus by a fixed amount at each temperature increment, allowing some equivalent transient strain to develop at constant load levels. Historically this formulation has been shown to give good results when comparing the results of calculations of the response of concrete elements in fire to the results of fire tests, but Anderberg however suggests that this is simply 'luck' that failure is predicted

using the implicit material model defined in the Eurocode [37]. Anderberg promotes the use of an explicit formulation of transient strain not directly coupled as an implicit factor in the stress strain model.

Nevertheless, for most applications involving reinforced concrete elements, where the compressive region is at the top of the element loaded in flexure the effective compressive preload in any concrete which will be heated is negligible so this ‘luck’ is perhaps not surprising. Further recent work has however highlighted that there are a number of cases whereby the role of the implicit transient strain model in the Eurocode is not necessarily suitable, most importantly where high levels of compressive load are present or where there is some cyclic nature to the loading, for example during cooling following a fire.

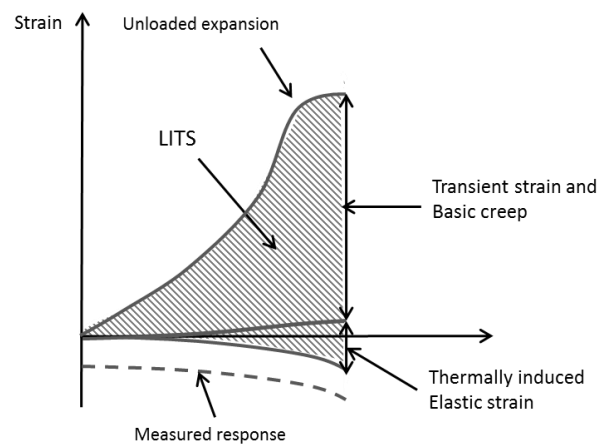


**Figure 2.1 – definition of LITS versus transient strain**

Gernay and Franssen developed an extension of the Eurocode 2 material model including an explicit transient strain component [38, 39]. In their study they reviewed the stress development at various points within a loaded concrete cylinder subject to heating and concluded that transient strain plays a significant role in the behaviour of loaded concrete specimens, especially during cooling. They concluded in their example that the residual axial load sustained by a column at the end of a fire comprising a heating and a cooling phase could be overestimated by up to 25% of the initial load if an implicit transient creep strain model is used.

Huang et al. presented an implementation of explicit transient strain in the Vulcan finite element software and studied the impact of transient strain on the buckling resistance of RC columns in fire [40]. It was found that the effect of including a formulation for transient strain in their model was significant and resulted in significantly reduced buckling times in fire.

In his thesis, Fellingner [30] discussed the impact of transient strain formulation on slip between the tendons and the concrete in finite element models of hollow core slabs. He compared the results of numerical modelling with test data when using an explicit transient strain formulation native to the DIANA finite element software (and based on work by Anderberg and Thelanderson [2]) with the results when using the concrete model in the Eurocodes [31] which includes an implicit component for transient strain. He concluded that the transient strain formulation plays a significant role in accurately predicting the response of hollow core slabs exposed to fire.

A comparison of a material model including an explicit and an implicit transient strain formulation was published by Lange and Jansson [41] where it was shown that for compressive loads of greater than approximately 30% of the compressive strength of concrete, the implicit transient strain formulation of the Eurocodes does not agree as well as explicit formulations. The explicit transient strain formulation which was chosen for this comparison and implemented in Abaqus via user subroutines was the same as that which is native to DIANA used by Fellingner [30].

Figure 2.2 shows a comparison between the results of finite element models of Anderberg and Thelandersons tests with constant load ratios of 0% to 67.5% under a constant heating rate of 5°C per minute. At 0% stress level, the Eurocode material formulation, Figure 2.2 a) agrees well with the test results although the Eurocode free thermal expansion is slightly higher than that determined in the tests. At 22.5% load level, the results also agree quite well, however with increasing load level the correlation between the strain response in the tests and the model becomes worse, and where the transient strain results in a negative net strain the Eurocode formulation does not capture this behaviour. Conversely, the explicit transient strain formulation agrees well at all load levels. Peak strains in the model occur at higher temperatures since the material tests which were used to define the stress strain response are of a different concrete mix. However the effect of transient strain on the net strain response correlates very well with the test results. To improve agreement between the tests and the analyses, the free thermal expansion in the explicit transient strain model, Figure 2.2 b), was modified to match the free thermal expansion in the tests, despite this the analysis of the difference between implicit and explicit formulation described above holds true.

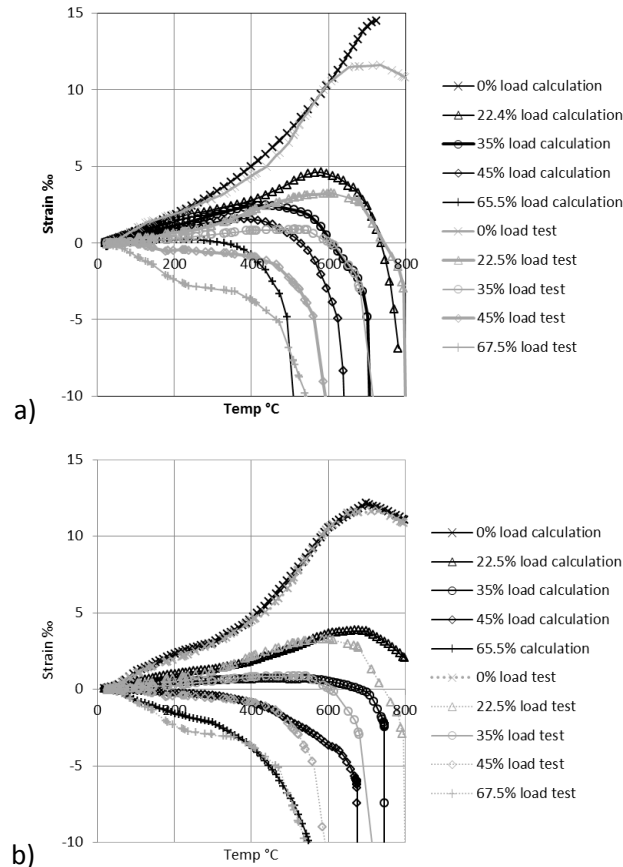


**Figure 2.2 – comparison between test results and finite element analyses of concrete cylinders under constant load heated at a rate of 5°C per minute, a) implicit transient strain model, and b) explicit transient strain model**

A subsequent evaluation of the impact of an explicit and an implicit implementation of LITS on prestressed concrete construction showed that the formulation had a significant impact on both the evolution of the prestressing force and the deflection history [41].

## 2.3 Application of transient strain model

In order to demonstrate the impact of the transient strain model to the response of hollow core slab elements, finite element modelling is carried out to study a series of fire tests conducted in Denmark in the 1990's [42].

### 2.3.1 Test details

In this series of tests, 3 slab sizes were subject to a standard fire, under 6-point loading. 2 slabs of each size were used in each test and were placed adjacent to one another although with no shear interaction as a result of screed on top of or grouting between the slabs. These tests were also modelled by Chang [26] using grillage models.

The tests are summarized here. Figure 2.3 shows the test setup in both plan and section. Figure 2.4 shows the geometry of the two slab cross sections.

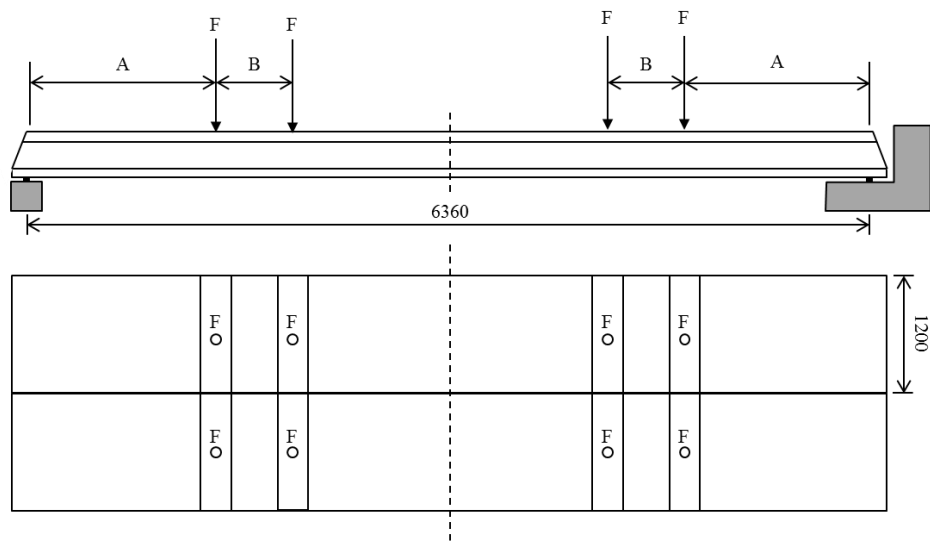


**Figure 2.3 – DIFT test setup plan and section, adapted from [42] (dimensions in mm)**

The section properties and load distributions are summarized in table 2.1. The magnitude of the loads shown in figure 2.3 and the distances between them are summarized in table 2.2.

**Table 2.1 –section properties and tendon area in the slabs**

<b>Section</b>	<b>Tendon diameter (mm)</b>	<b>Approx. area of concrete (mm<sup>2</sup>)</b>	<b>Prestressing load (steel) (kN per strand)</b>
SP18	9.3	146 150	58
SP22	9.3	159 280	58
SP27	12.5, 15.2	178 030	104, 138

**Table 2.2 – load configuration of the tests**

<b>Section</b>	<b>Prestressing load (kN)</b>	<b>A (mm)</b>	<b>B (mm)</b>
SP18 and SP22	16.93	1084	1200
SP 27	28.02	1600	1000

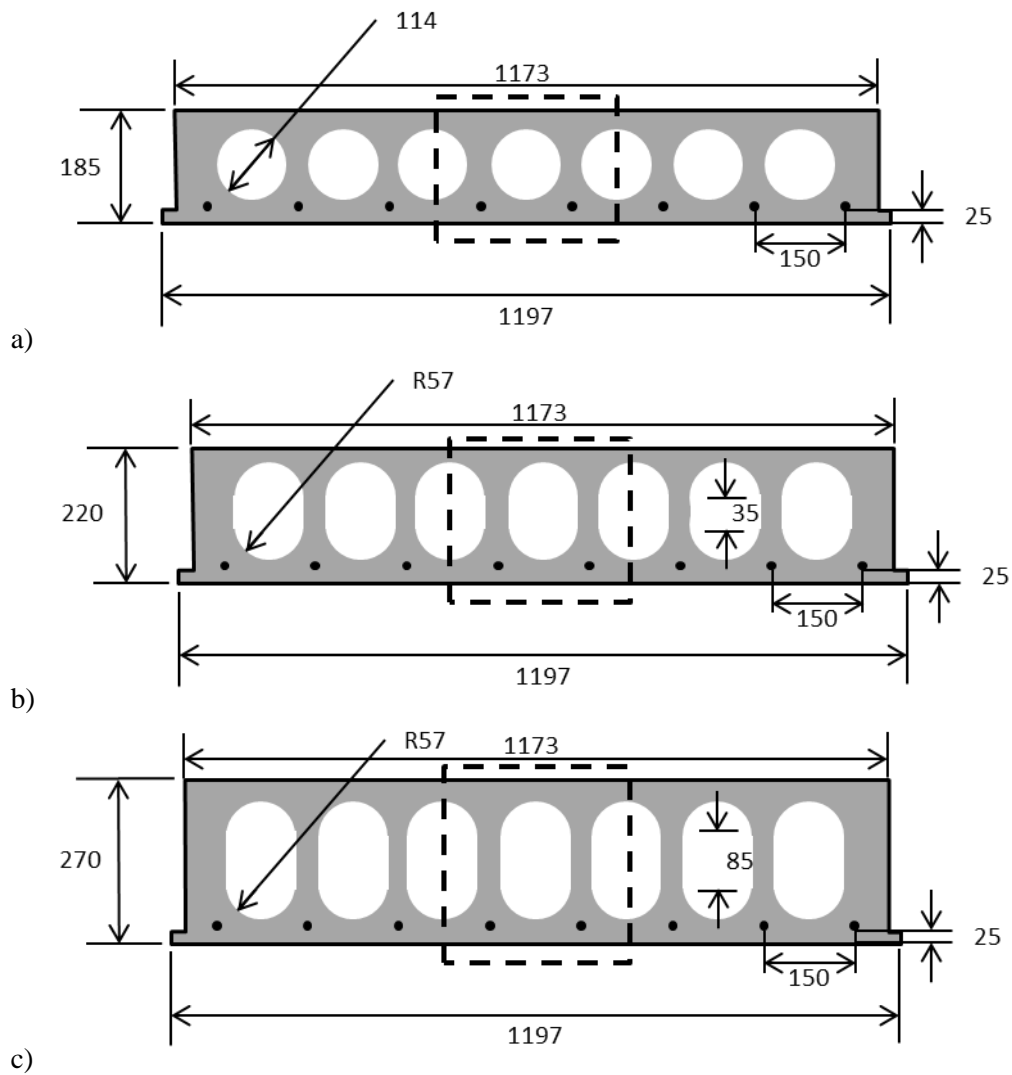


**Figure 2.4 – dimensions (in mm) of the hollow core slab sections (modified from [42]), a) SP18 slab section, b) SP22 slab section, and c) SP 27 section (the dashed region indicates the area which is modelled in this section)**

### 2.3.2 Numerical modelling

Thermal modelling of all three slab sections was performed and the explicit transient strain model was used in a mechanical model the smallest two of the slab sections. This allowed a comparison between the results of modeling using the explicit transient strain model with that of modeling carried out using an implicit transient strain model. The 2 slab sections which are studied further were subject to the same loading conditions resulting in different utilization factors of the slabs, as in the tests.

Numerical modeling was carried out using the Abaqus finite element program version 6.14-1. For all three slabs, a heat transfer analysis was carried out using the standard solver and the mechanical analysis in the smallest two slab sections was carried out using the explicit solver, with the results of the heat transfer analysis applied to the concrete solid elements as a field variable during the heated step of the mechanical analysis. Prestressing tendons were not included in the thermal calculation and the temperature of the tendons was assumed to be equal to the temperature of the concrete in the thermal analysis at the location of the bottom of the tendons, accounting for a high conductivity of steel, i.e. where the tendons were closest to the heated surface of the concrete.

### 2.3.2.1 Heat transfer analysis

In both the heat transfer analysis and the mechanical analysis the slab model represented a slice of the slab comprising one hollow core and the two webs on either side plus half of each of the cores on either side, as indicated by the dashed lines in Figure 2.4. The model was a total of 3.18m in length, spanning 3.1m from the line of symmetry at mid span to the support, with an exposed length of 3m from the line of symmetry and an overhang of 8 cm.

In the heat transfer analysis of the SP18 slab section, a total of 39 856 solid 8 noded heat transfer finite elements were used to model the concrete, with temperature dependent heat transfer properties chosen according to Eurocode 2, using the upper limit of thermal conductivity. In the SP22 slab, 44 944 elements were used. Thermal loading was applied to the exposed surface of the concrete slab only in the form of an ISO fire curve. A surface film interaction was used for the convective heat transfer, with a convective heat transfer coefficient of  $25 \text{ W/m}^2\text{K}$ . Radiative heat transfer was based on a surface emissivity of 0.8, which is conservative compared with the requirements of EN 1992 [32]. On all unexposed surfaces (except those which represented a line of symmetry or continuity of the slab), ambient temperature conditions were applied in the same way, with a convective heat transfer coefficient of  $5 \text{ W/m}^2\text{K}$  and a surface emissivity of 0.8. Figure 2.5 shows the finite element mesh of the three different slabs for the thermal analysis.

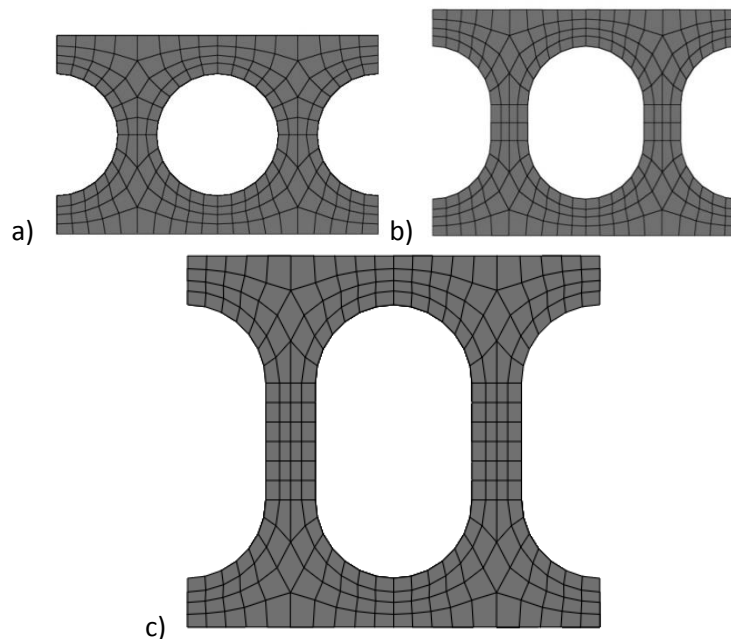


**Figure 2.5 – finite element mesh of the concrete in the hollow core slabs; a) SP18 section, b) SP22 section, c) SP 27 section**

The heat transfer calculation had a duration of fire exposure of 30 minutes. Figures 2.6 a) through c) show the through depth temperatures through one of the webs of each of the slabs at various times during the heat transfer calculation. All temperatures shown are in K.

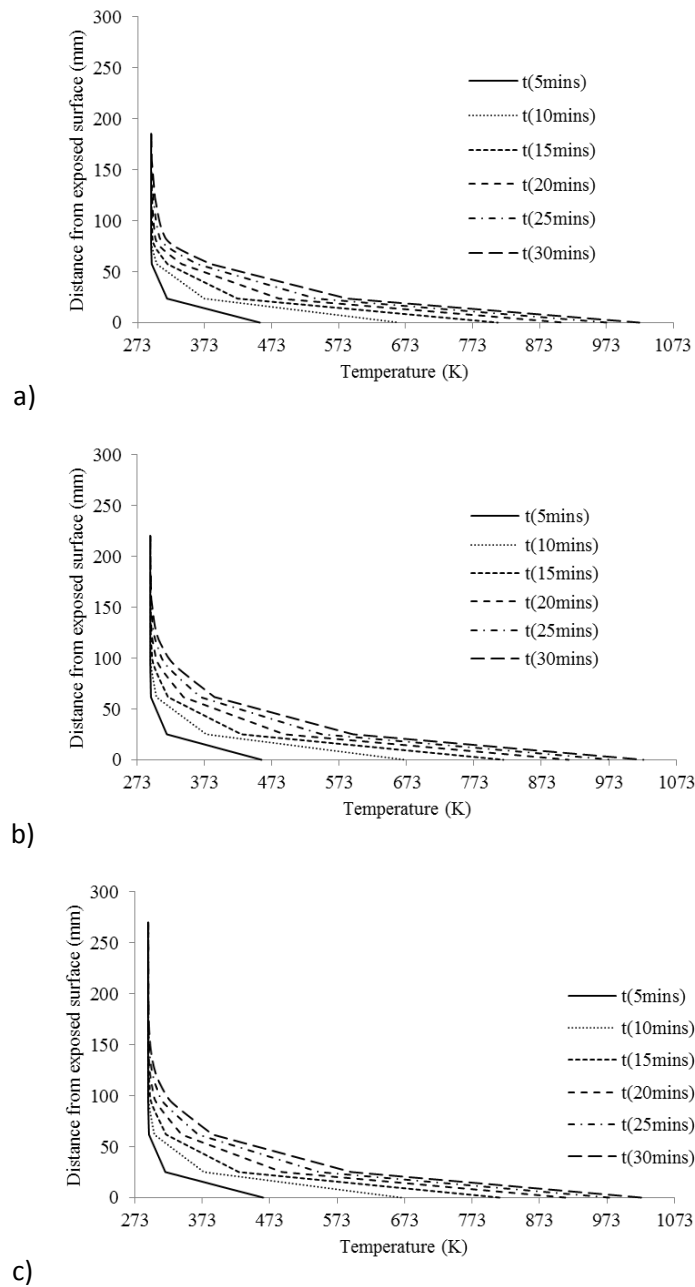


**Figure 2.6 – through depth temperatures through the centre of the web of the slabs at different times; a) SP18 section, b) SP22 section, c) SP 27 section**

### 2.3.2.2 Mechanical analysis

The mesh representing concrete in the mechanical analysis was identical to the mesh in the heat transfer analysis. Prestressing tendons were modeled using solid elements as embedded regions in the solid concrete mesh. The reason for using solid elements was to prevent potential problems with hour glassing in the concrete as a result of localization of loads if beam or truss elements were used instead. Prestressing in the form of a uniform predefined field was applied as an initial condition to both the concrete part and the tendons. All tendons in the modelling were prestressed with a mechanical load of 62kN per strand, as per the design of the concrete elements in the tests. Mechanical load was applied in the first step of the mechanical analysis during which time the prestressing load was allowed to equilibrate. The release of the prestress at the start of the analysis resulted in some dynamic effects in the analysis affecting the vertical displacement of the models.

These were reduced by applying a small amount of material damping ( $\alpha=0.06$ ) to the concrete material in the model.

The Abaqus Concrete Damaged Plasticity model was used for concrete in the model with the material stress strain curves in compression derived from the expression in Eurocode 2 part 1-2 using either the temperature dependent reduction factors and strain values stipulated in the code or the model described and referenced in section 2.2, above. The resulting stress strain curves of concrete are shown in Figure 2.7.

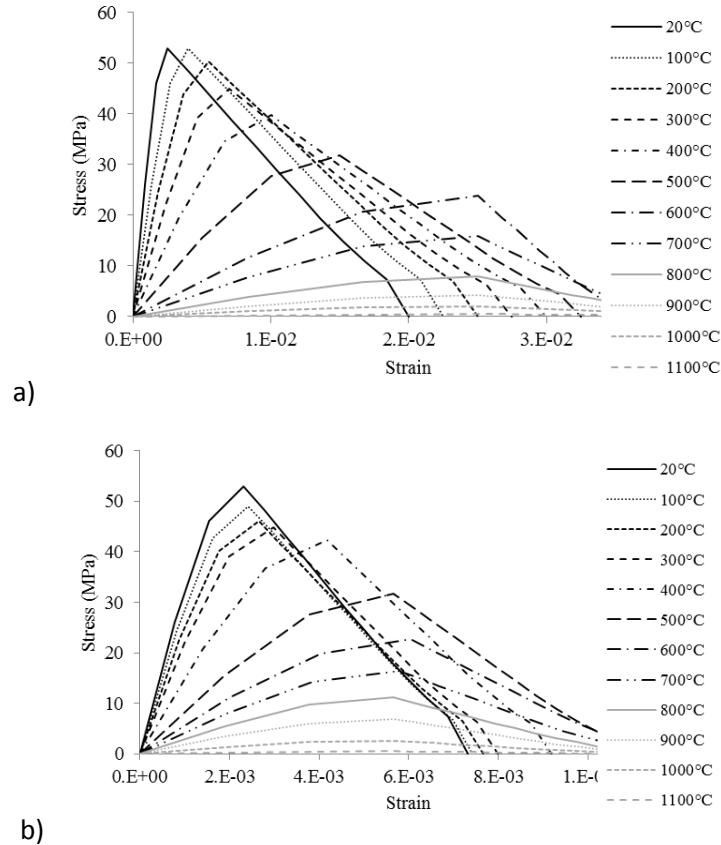


**Figure 2.7 – stress strain curves of concrete in compression for concrete with a compressive strength of 53MPa; a) eurocode material properties, and b) material properties derived from tests reported in literature [39]. Note the different scales of the x-axis**

For the tensile behavior of the concrete a fracture energy of  $0.21 \text{ Nmm/mm}^2$  was used. This is higher than the values given in the CEB-FIP Model code of  $0.025$  to  $0.058 \text{ Nmm/mm}^2$  depending upon the aggregate size [43]; however this was done in order to improve stability of the model. Law reviewed the impact of increasing fracture energy in models of reinforced concrete and concluded that it made little difference to the final result in terms of deflections of the model [35]. The variation in tensile strength with temperature was assumed to be the same as the variation in compressive strength with temperature in Eurocode 2 part 1-2, with the peak tensile strength at ambient temperature equal to 10% of the compressive strength. Tensile strength is shown in Figure 2.8 plotted against temperature. Unlike the compressive strength, it was not varied between the implicit and explicit material models.

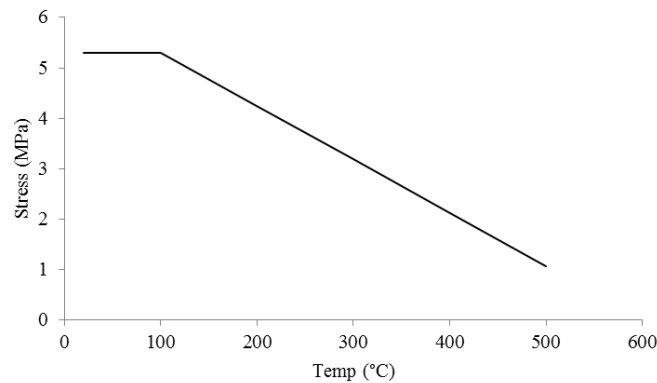


**Figure 2.8 – variation in tensile strength of concrete with temperature**

Steel for the prestressing tendons was assigned the material properties in Eurocode 2 part 1-2. As reported from the tests the stiffness was 200 000 MPa. The 0.1% proportional limit was 1 600MPa and the yield stress was 1 800MPa. Strength and stiffness were varied with temperature according to the Eurocode. The stress strain curves for various temperatures are shown in Figure 2.9.

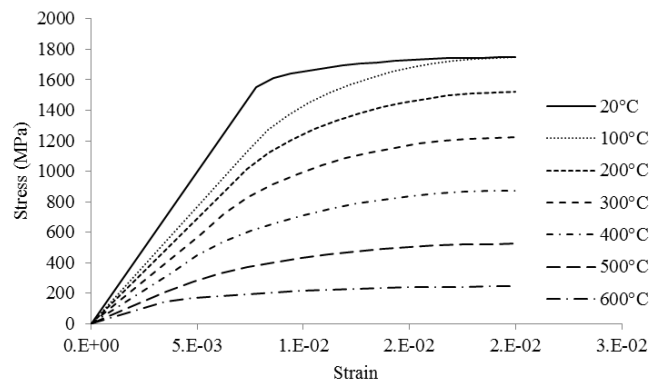


**Figure 2.9 – stress strain curve of the prestressing steel at various temperatures**

Mechanical restraint was provided in the form of a restraint of the model in the global y-direction only at one end, 80mm from the heated region; and as a symmetry boundary condition at the mid-span of the slab element.

Following application of the mechanical load, the temperatures in the slab and the prestressing tendons were added in the form of field variables in an additional step. The whole heat transfer analysis was time scaled in the explicit mechanical model by a factor of 1000 to reduce run times and no rate dependent material properties were used in the model. Each of the models was run using both the Eurocode material properties and the material properties discussed above, i.e. using both the implicit and the explicit transient strain material model.

The abaqus explicit solver is used for the mechanical analysis. Since the transient strain is dependent upon the stress level in the material this strain component is not isotropic in the cross sections investigated. Abaqus explicit allows anisotropic or orthotropic thermal expansion coefficients to be defined through the use of the VUEXPAN user subroutine. In order to simplify the analysis, the implementation of transient strain as a component of an isotropic thermal expansion in the material definition is achieved by linking the maximum principle stress in the direction of span of the slab with the field variable which

defines the transient strain using the VUSDFLD user subroutine. It is therefore assumed that transient strain is isotropic in the calculation. This means that the total strain in the lateral direction, orthogonal to the span of the slab will include the same transient strain as the expansion in the longitudinal direction, affecting results in this direction. However, since the model is representative of only a small portion of the width of a hollow core slab it is not expected that this will have a significant impact upon results.

## 2.4 Results

Results are presented in this section for both the SP18 and the SP22 slab sections. In particular, focus is placed on the difference in the response of the prestressing tendons during the test – comparing the two implementations of transient strain described. Validation of the models is carried out through comparison of the deflections from the models with the deflections which were observed in the tests.

### 2.4.1 SP18 Slab

Figure 2.10 shows a comparison between the deflections of the SP18 slab models with the results reported for the test. In the test, one of the 2 slabs failed after approximately 1300 seconds at which time the test was stopped. In the model which utilized the implicit transient strain formulation the deflections which were observed at the end of 30 minutes of heating were nearly double the deflections which were observed in the tests. Deflections early on during heating in fact rise, quite probably as a result of the lower stiffness of the heated concrete in the lower flange and the result this has on the eccentricity of the prestressing load on the effective cross section. At the end of heating, the model which utilized the explicit transient strain formulation had undergone deformations approximately equal to the deformations in the test at the time of failure. At the time of failure of the test specimens the two numerical analyses differ by approximately the same amount, the implicit transient strain model shows a higher deflection than the test result by approximately 50mm whereas the explicit transient strain model shows a lower deflection by about 75mm.

There are two aspects to consider which contribute to the change in deflection between the two models, both driven by the reduction in initial tangent modulus in the implicit transient strain formulation:

- First of all, the reduction in material stiffness with increasing temperature reduces the rigidity of the element with increasing temperature. This results in higher mechanical deflection resulting from the applied loading.
- Secondly, the reduced contribution to the thermal curvature as a result of a lower stiffness at higher temperatures.

Clearly there is some interaction between these two effects which contribute in different ways to the global response of the two models. Nevertheless, it may be considered that the deflection results are not unreasonable and the trend in both models correlates with the experimental results (i.e. an almost linear increase in deflection, no indication of impending runaway).

Aside from the deflections, no additional data is reported for this test and so no further comparison between the numerical results and experimental results is possible.

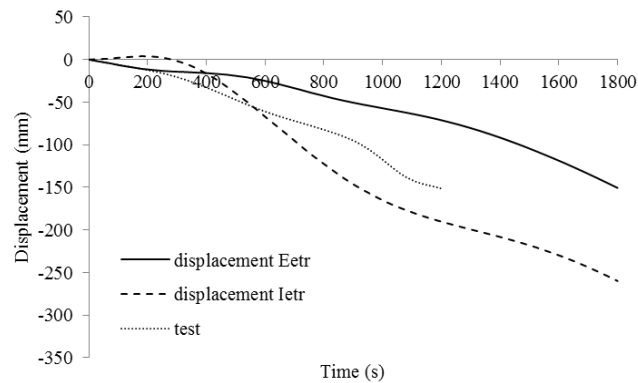


**Figure 2.10 – deflections of the SP18 slab models and test results the series ‘displacement Eetr’ and ‘displacement Ietr’ denote the results of the models with explicit and implicit transient strain material model respectively**

Figure 2.11 shows the stress in the prestressing tendons, derived solely from the numerical model. This is derived from the stress in the global y-direction of the model, averaged for all elements which comprise the prestressing tendons at the mid-span of the beam. There is a clear difference in the behaviour of the tendons in the two models, with an increase in stress shown in the model with an implicit transient strain formulation. This is most likely a result of the downwards deflection of the slab, which is higher in this model than in the test and the model with the explicit transient strain formulation. The increasing deflection results in an increasing tensile load acting on the prestressing tendons. With increasing time, the prestressing tendons begin to heat up and the effect of thermal expansion begins to relieve the prestressing force. This second effect is clearly dominant in the model with explicit transient strain, where the increased deflections were smaller and the increase in tension as a result of this is only dominant in the early stages of the fire. After approximately 300 seconds the stress begins to reduce. Once the effect of increasing temperature begins to dominate over deflection in the Eurocode model, the stresses run almost parallel to one another.

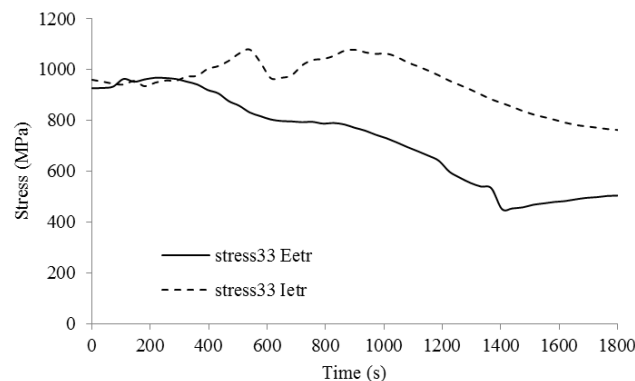


**Figure 2.11 – stress in the tendons of the SP18 slab models the series ‘stress33 Eetr’ and ‘stress33 Ietr’ denote the results of the models with explicit and implicit transient strain respectively**

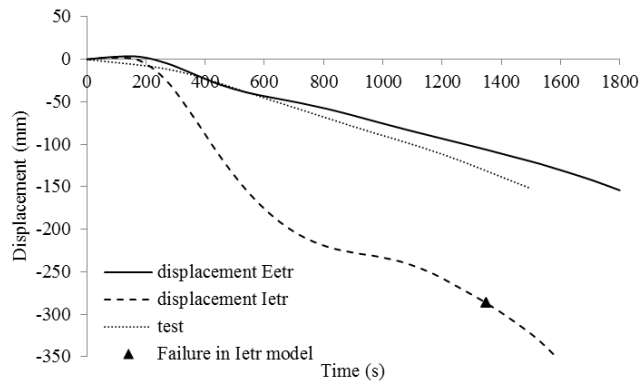
#### 2.4.2 SP22 Slab

In the mechanical model of the second slab, a large plastic strain indicative of shear failure along the web of the slab at the support was observed in the model with implicit transient strain. This occurred at around 1350 seconds into the analysis and was followed

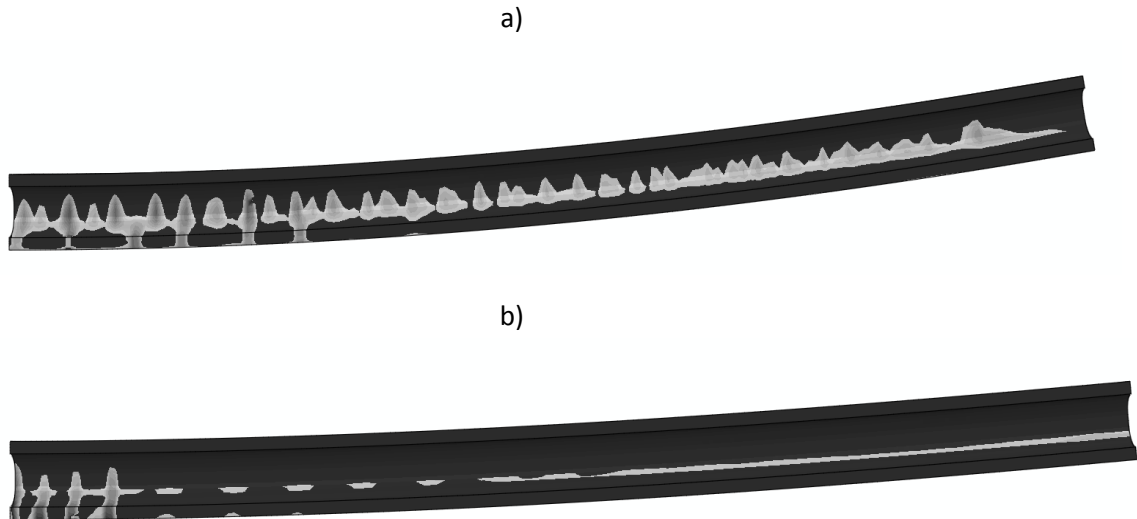
by an increased rate of deflection of the floor slab. One of the two test specimens failed after 1560 seconds, although this was a result of a combination of shear and bending in the slab rather than shear along the web as in the model.

A comparison of the deflections of the models with an implicit and an explicit formulation of transient strain with the test results is shown in Figure 2.12. The results of the numerical analysis with the explicit transient strain formulation agree very well with the test results, whereas the model using the Eurocode material properties shows poor agreement. The failure time and deflection of the model which used the Eurocode material properties is also indicated on the figure.

Although the Abaqus concrete damaged plasticity model does not track crack growth explicitly, the development of cracks may be indicated by areas of high plastic strains. Figure 2.13 shows a comparison between the crack patterns which were seen in the two slab models as a visualization of the compressive plastic strain in the models. No description of cracking is given in the test report, however the patterns which are seen in the numerical models agree well with the patterns which are observed by and described by, e.g. Fellingner[30]. The degree of cracking in the model with an implicit transient strain formulation is significantly higher than the model with an explicit formulation.



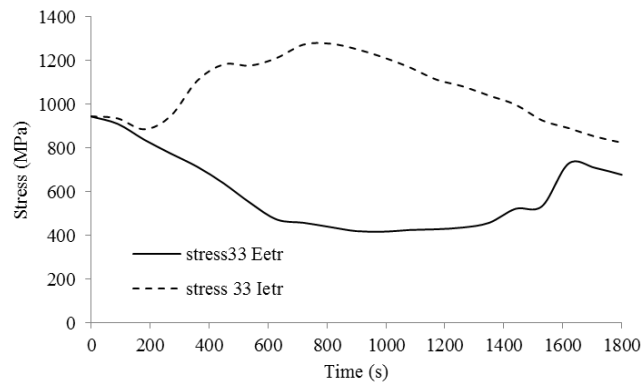
**Figure 2.12 – displacements of the slab in the models and in the test, the triangle symbol indicates the time and displacement in the numerical analysis where plastic strains indicating model shear failure occurred in the web in the implicit transient strain model**



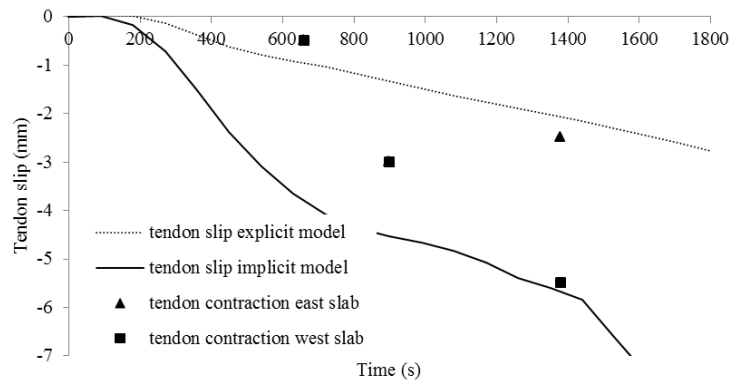
**Figure 2.13 - Crack patterns plotted on the deflected shape for the SP22 slab modeled using an implicit (a) and an explicit (b) transient strain formulation**

Figure 2.14 shows the stress in the tendons at the midspan for each of the models. Once more, the implicit transient strain model shows a general increase in the stress in the tendons during the early phase of the fire, coinciding with an increase in the deflection in the model. This stress increases until approximately 800 seconds when the effect of reduction of prestress by thermal expansion begins to dominate. The model with the explicit transient strain formulation however shows a general decrease in the stress in the tendons as the analysis progresses, with the effect of thermal expansion dominating over any increase in mechanical stress induced by increasing deflection. Increasing deflection in this model does lead to an increase in the mechanical stress after approximately 1200 seconds of analysis, however up until this time the prestressing force has reduced by over 50%.

Also reported in the observations from this test were the contraction of the strands from the free end of the concrete slabs. No indication is given as to how this was observed, however it is interesting to compare the slip in the tendons at the ends of the slabs during the analysis with the values which are quoted. During the test, the west most slab was the one which failed, and this was observed to have the most slip in the tendons, 5-6 mm at the end of the test. In the slab which did not fail the slip at the end of the test is reported to have been between 2 and 3 mm. Figure 2.15 shows a comparison between bond slip reported for the test for the two slabs and the bond slip from the numerical analyses, where the bond slip was determined as the horizontal distance between the free end of the concrete and the end of the prestressing tendon. The bond slip defined in this way in the numerical model with explicit transient strain agrees very well with the final value reported for the slab which did not fail (the east slab). A comparison with the bond slip in the slab which did fail shows very good agreement with the numerical model with implicit transient strain. However this is nothing more than a coincidence since the time of the final reported measurement of tendon contraction in the test coincided almost exactly with the final failure of the slab.



**Figure 2.14 – stress in the prestressing tendons during the fire exposure in the models using the implicit and the explicit transient strain model**



**Figure 2.15 – tendon displacement (slip) in the models. The symbols indicate the observations made during the test**

## 2.5 Discussion

In both of the models of the SP18 section slab, the general trend of the numerical deflections agrees fairly well with the reported test deflections, although the model with explicit transient strain underestimates the deflections, by as much as 50 %; and the model with the implicit transient strain formulation overestimates the deflections by as much as a third. The numerical analysis of the SP22 slab which included the explicit transient strain material formulation showed far better agreement ; however the difference in deflection between the reported deflections for the SP22 slab and the numerical model with the implicit formulation of transient strain is significant. In both cases, the models with the implicit formulation of transient strain gives a higher deflection than the test results whereas the model with the explicit formulation gives a closer approximation in the case of the SP22 slab.

The explicit transient strain model is also shown to give a very good estimation of tendon contraction at the free ends of the slab. Altogether, the comparison between the tests and the numerical results lend support to the validity of this model, although more work is clearly needed.

The impact of transient strain formulation on the stress in the prestressing tendons has been shown to be significant, with increased deflection observed in the models with the implicit transient strain formulation leading to significant increase in the stress in the

prestressing tendons. This increase in mechanical stress offsets the effect of loss of prestress as a result of heating of the prestressing tendons.

The conclusions from the test report [42] offered some discussion on the relatively low failure times of the hollow core slabs in the tests. In all of the slabs, failure occurred in the region of the supports and does not appear to have been caused by bending. Anchorage failure, as well as shear capacity were not correctly predicted, but the temperature of the reinforcement was very low at the time of failure (100 – 150 °C), suggesting that the reduction factor for these capacities was close to unity. Because of the very early failure times in these tests in comparison with other tests, expected fire resistance times, or real failures as described above, it was decided to base the subsequent work in the project on analytical methods. Such an approach, while also requiring validation allows a quick and simpler method for making comparisons about the effect of different choices made in the design of these elements.

## 3 Analytical modelling of prestressed concrete construction

### 3.1 Introduction

In order to evaluate the effect of different variables on the response of prestressed monolithic and hollow core concrete construction, an analytical approach was developed and is described here. This has the advantage, compared with the numerical modelling, of allowing several different variables to be studied quickly to evaluate the influence of parameters such as concrete strength and stiffness, cross section geometry, tendon placement and tendon prestress. However, it has the disadvantage of not being able to capture the nuances of the behaviour which numerical modelling can achieve. Nevertheless it is proposed here as a screening method for studying the effects of these different parameters.

The proposed approach relies on an extension of previously validated analytical expressions for the description of structures in fire, e.g. [44]. The analytical methodology described here was implemented in MATLAB.

### 3.2 Methodology

The methodology comprises 4 main phases: a heat transfer analysis followed by the determination of the thermal strains and the impact of the reduced stiffness of the heated regions on the cross section (a calculation of an equivalent cross section based on a reference stiffness which has the same properties as the heated cross section), an adjustment of the prestressing force based on the temperature of the tendons, a calculation of the ultimate moment of the cross section accounting for the temperature dependent properties of the concrete and the tendon as well as the thermal strain in the concrete. The method is shown schematically in Figure 3.1.

Based on the results up to stage 3 in the analysis, the thermally induced displacements of a prestressed concrete section could also be determined. This will give an indication of the required bearing width required to support prestressed construction.

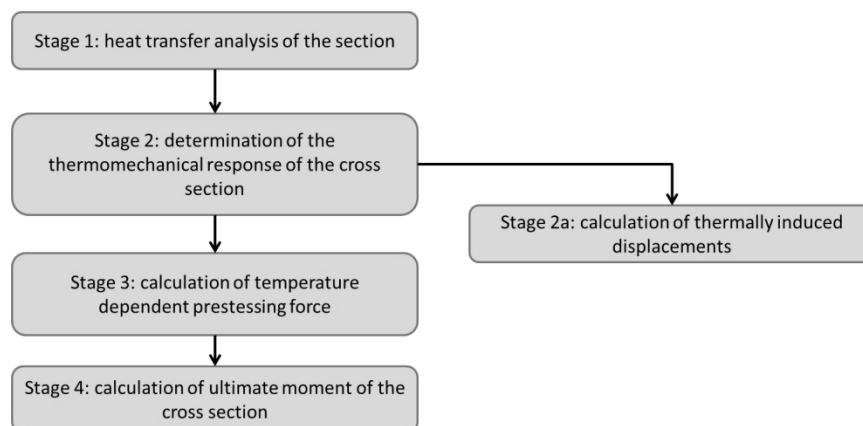


**Figure 3.1 – main stages in the analysis method for prestressed concrete construction**

### 3.3 Heat transfer analysis

The heat transfer analysis of hollow core slabs which is required for the analytical method is exactly the same as the heat transfer analysis which is described in the previous chapter. In the examples which are given, the temperatures are averaged across the width of the hollow core section rather than being taken at the centreline of one of the webs. This will lead to a slightly larger temperature in the region of the tendon, most likely leading to a conservative analysis.

For monolithic prestressed concrete construction a simple one dimensional analytical or finite element heat transfer analysis could be undertaken. In the comparisons which are shown in this section a one dimensional finite element heat transfer analysis was undertaken

### 3.4 Thermo-mechanical response of the cross section

In order to determine the response of composite and concrete slabs to heating through the cross section in structural fire engineering it has been proposed in the past to idealise the temperature distribution through the section as a mean temperature increase and an equivalent uniform thermal gradient [45, 46, 47]. This method is implemented here since it allows the equivalent thermal gradient and equivalent temperature increase, as well as the overall response of the section, to be estimated based on a single reference value of the stiffness.

The thermal gradient is evaluated using a method detailed in [45], which was developed for the analysis of composite sections. The method is based on a similar method for determining the effects of temperature on composite bridge decks and is summarised here to aid discussion. Figure 3.2 shows the division of an arbitrary section, subject to one dimensional heating, into  $n$  slices along with an estimation of the temperature of each slice and the temperature dependent material properties of each slice.

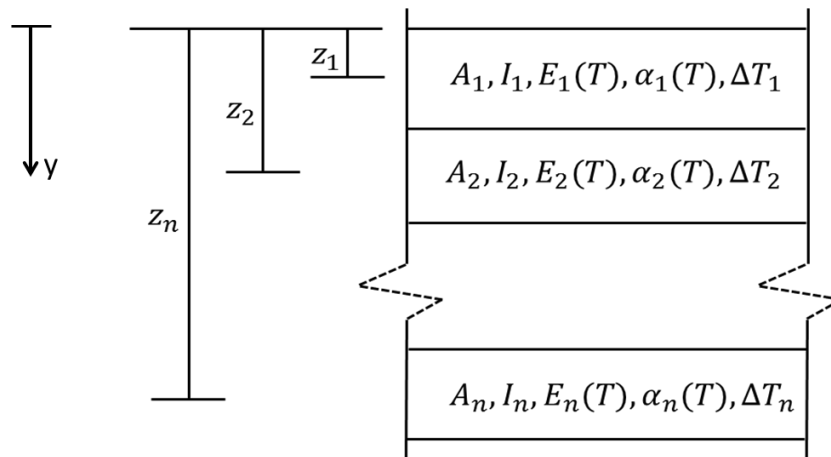


Figure 3.2 – The division of an arbitrary section into slices, adapted from [45]

Each slice,  $i$ , has temperature dependent material properties, and a distance,  $z_i$ , to its neutral axis measured from an arbitrary reference position,  $\bar{z}$ , on the major axis. The resultant thermal force and thermal moment in a fully restrained section arising from the temperature increase in each slice is determined from:

$$F_T = \sum_{i=1}^n E_i A_i \alpha_i \Delta T_i \quad (3.1)$$

$$M_T = (F_T \times \bar{z}) - \sum_{i=1}^n F_i z_i \quad (3.2)$$

Where  $F_i$  is the thermal force in slice  $i$ , given by  $F_i = E_i A_i \alpha_i \Delta T_i$ . As described by Usmani and Lamont, the second moment of area of the section is based on the parallel axis theorem with the contribution of each of the area's corrected by a suitable modular ratio to a given reference modulus. This gives a second moment of area of the heated section about the major axis:

$$I = \sum_{i=1}^n I_i/m_i + A_i/m_i (z_i - \bar{z}) \quad (3.3)$$

Where  $I_i$  and  $A_i$  are the second moment of area and the area of the slice  $i$  respectively, and  $m_i$  is the ratio of the temperature dependent modulus of elasticity of the slice to the reference modulus. A similar procedure may be used to find the effective area of the section:

$$A = \sum_{i=1}^n A_i/m_i \quad (3.4)$$

Because each of the slices has a different temperature and the coefficient of thermal expansion is dependent upon the temperature, the net coefficient of thermal expansion of the section must also be modified appropriately based upon the contribution of each of the slices. This is done by averaging the expansion over the total area, accounting for the modular ratio:

$$\alpha = \frac{1}{A} \sum_{i=1}^n \alpha_i A_i/m_i \quad (3.5)$$

Finally, the total thermal strain  $\varepsilon_T$ , curvature  $\phi_T$  and the equivalent temperature increase  $\Delta T$  and equivalent thermal gradient,  $T'_x$  on the section may be determined from the following equation based on the reference stiffness:

$$\varepsilon_T = F_T / E_{ref} A; \text{ and } \Delta T = \varepsilon_T / \alpha \quad (3.6)$$

$$\phi_T = M_T / E_{ref} I_{tot}; \text{ and } T'_x = \phi_T / \alpha \quad (3.7)$$

To illustrate the temperature gradient, average temperature increase as well as the thermal moment and thermal force in a section, the methodology described above is applied to three different hollow core slabs. These are the same hollow core slabs which were used in the tests described in the previous chapter, the geometry of which is shown again in Figure 3.3. For the method described, the hollow core slabs are reduced in width to consider one representative web, in the middle of the cross section from the vertical centreline of one core to the vertical centreline of an adjacent core. The dashed line in Figure 3.3 indicates the region which is represented by this method, which is different from the region considered in the finite element modelling in the previous chapter. For the comparison, the monolithic prestressed concrete slabs are assumed to be of equal

width to the area of the hollow core slab considered and to only contain one tendon, located in the same place as for the hollow core slab section. The resulting cross section for the monolithic examples is then the same height as the hollow core slabs shown in Figure 3.3, but is the same width as the area delimited by the dashed lines.

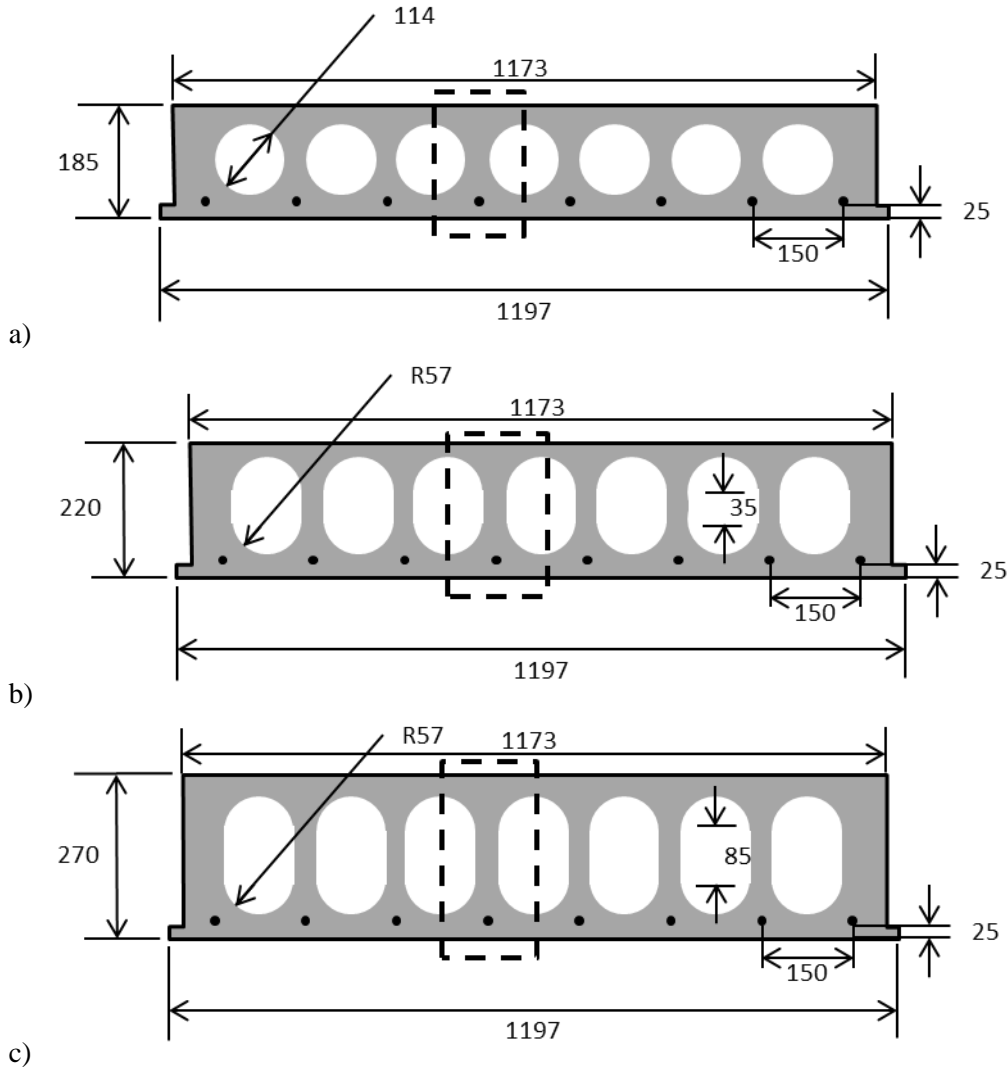


**Figure 3.3 – Hollow core slab sections a) SP 18, b) SP22, and c) SP27 (the dashed region indicates the area represented in the analytical model)**

For the analyses, the concrete is assumed to have a stiffness at ambient temperature of 31 500 N/mm<sup>2</sup>, based on the initial tangent modulus of the concrete compressive stress strain curve. This is also used as the reference stiffness for the concrete throughout. Temperature dependent stiffness is based on the temperature dependent stress strain curves in Eurocode 2 [29], i.e. the curves with the implicit transient strain formulation. The stiffness is based on the initial tangent modulus of the stress strain curve at different temperatures.

The equivalent thermal gradient and temperature increase are shown in Figures 3.4 and 3.5 respectively. Comparison between the hollow core slabs and the monolithic concrete slabs of the same thickness shows a significant difference in both the thermal gradient and the equivalent average temperature increase. In all three cases the hollow core slabs have higher values of both thermal gradient and equivalent temperature increase. This is because the cores reduce the thermal bulk diffusivity through the specimen, forcing energy to be retained in the lower flange, increasing the temperature in this region and the

thermal gradient. In all three examples shown the maximum thermal gradient reduces with increasing thickness of the hollow core slabs, whereas the maximum equivalent temperature increases.

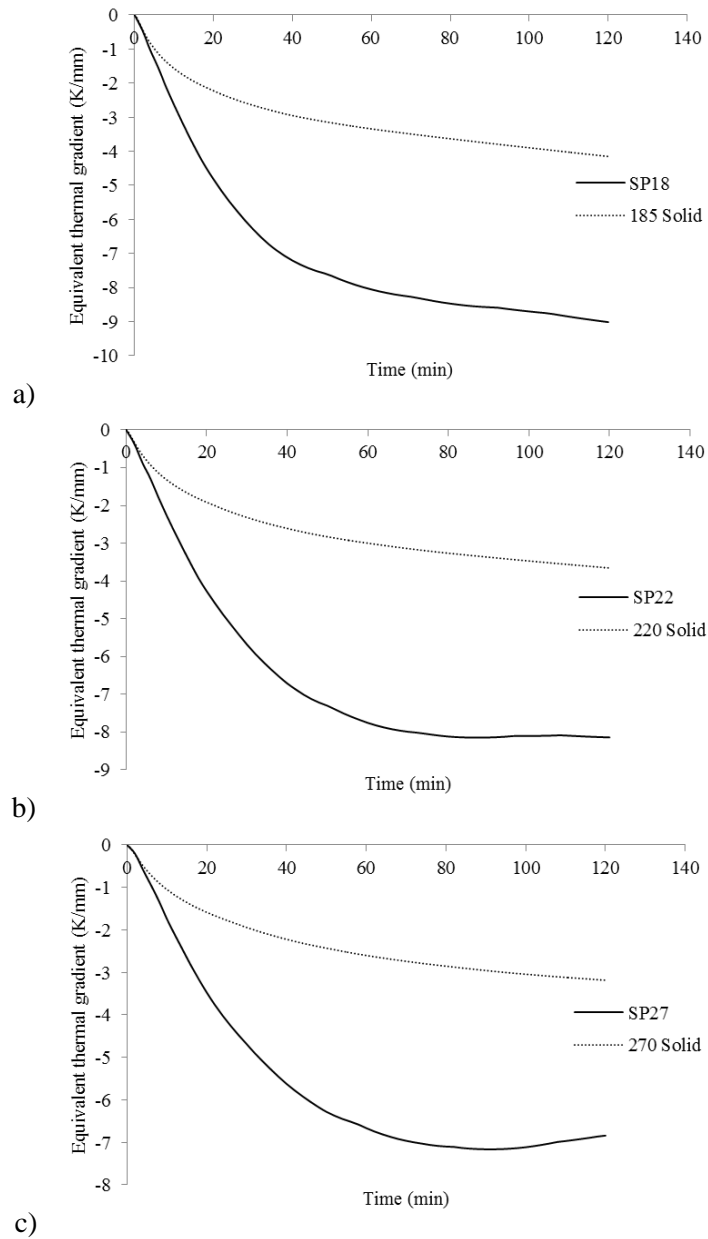


**Figure 3.4 equivalent uniform thermal gradient, as defined in equation 3.7 in a) the SP 18 hollow core slab and a 185 mm deep concrete slab b) the SP 22 hollow core slab and a 220 mm deep concrete slab and c) the SP 27 hollow core slab and a 270 mm deep concrete slab**

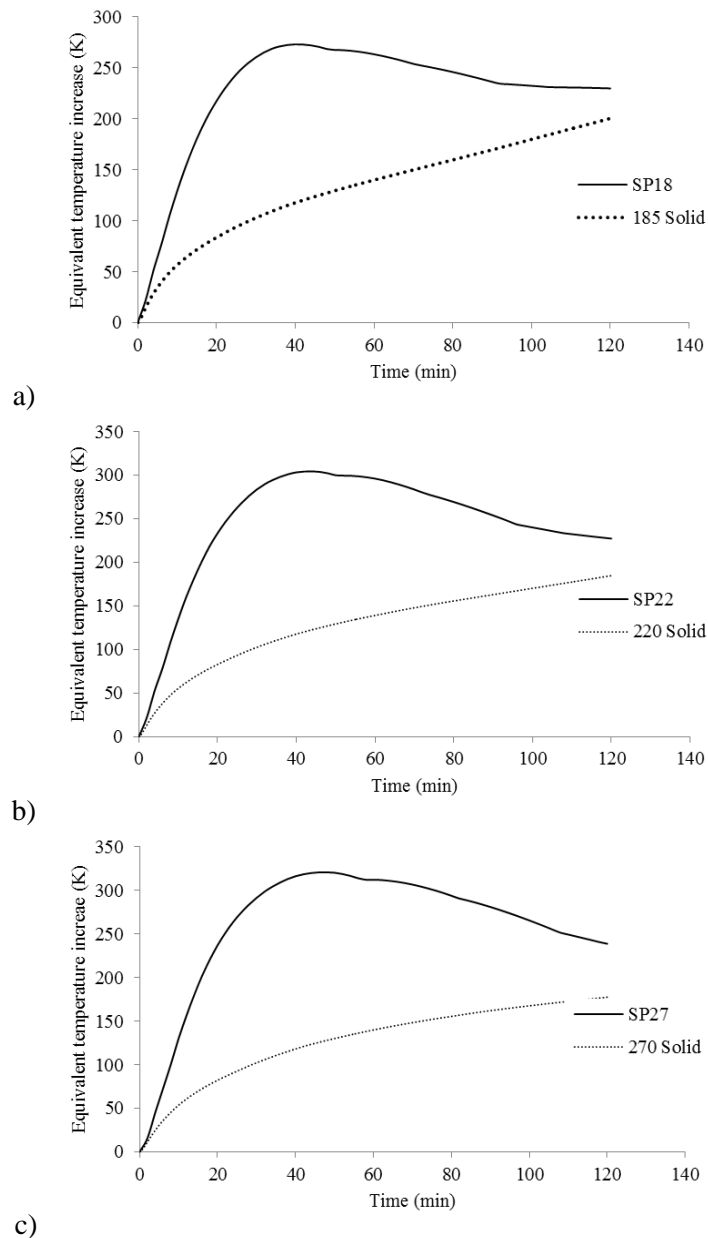


**Figure 3.5 - equivalent temperature increase, as defined in equation 3.6, in a) the SP 18 hollow core slab and a 185 mm deep concrete slab b) the SP 22 hollow core slab and a 220 mm deep concrete slab and c) the SP 27 hollow core slab and a 270 mm deep concrete slab**

The resulting thermal moments and thermal forces in the same sections are shown in figures 3.6 and 3.7. The magnitudes of both the thermal moment and the thermal force in the hollow core and the monolithic sections increases with increasing thickness of the section. However, the ‘trapping’ of heat in the lower flange of the hollow core flange sections and the effect of this on the equivalent section means that there is a peak thermal moment and a peak thermal force in the hollow core slab sections at around about 1 hour of fire exposure, whereas the monolithic specimens continue heating.

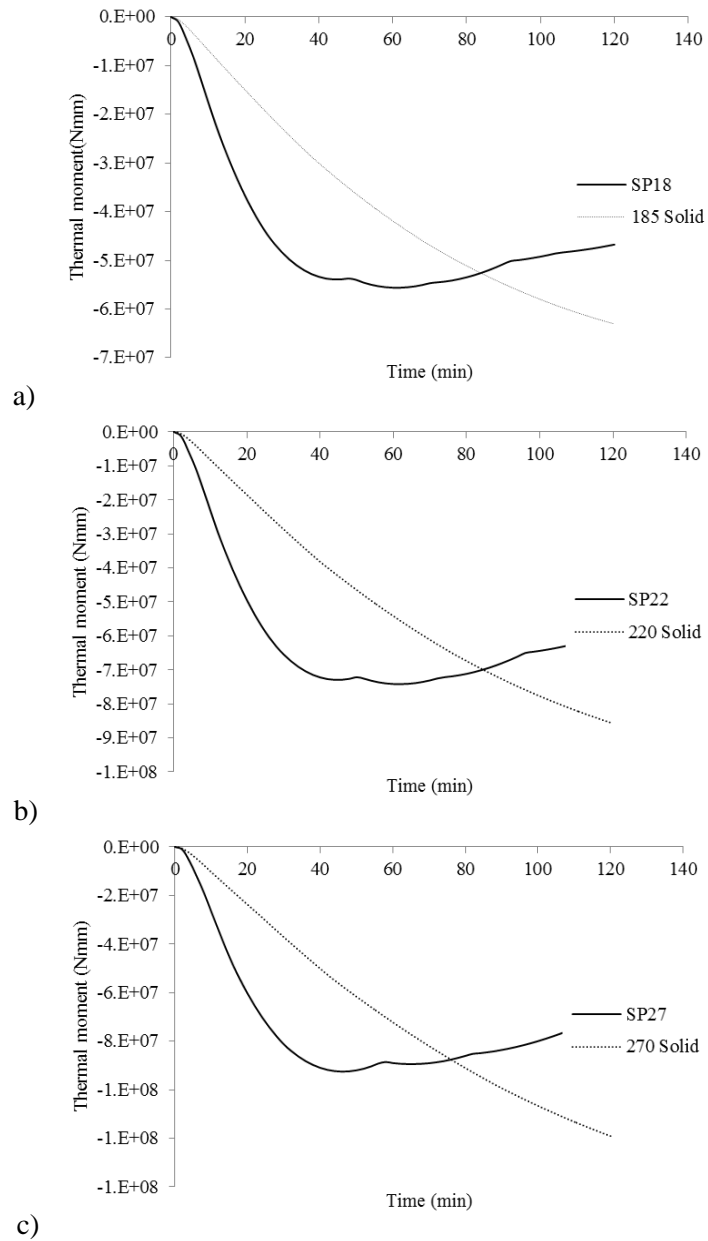


**Figure 3.6 – thermal moment, as defined by equation 3.7, in a) the SP 18 hollow core slab and a 185 mm deep concrete slab b) the SP 22 hollow core slab and a 220 mm deep concrete slab and c) the SP 27 hollow core slab and a 270 mm deep concrete slab**

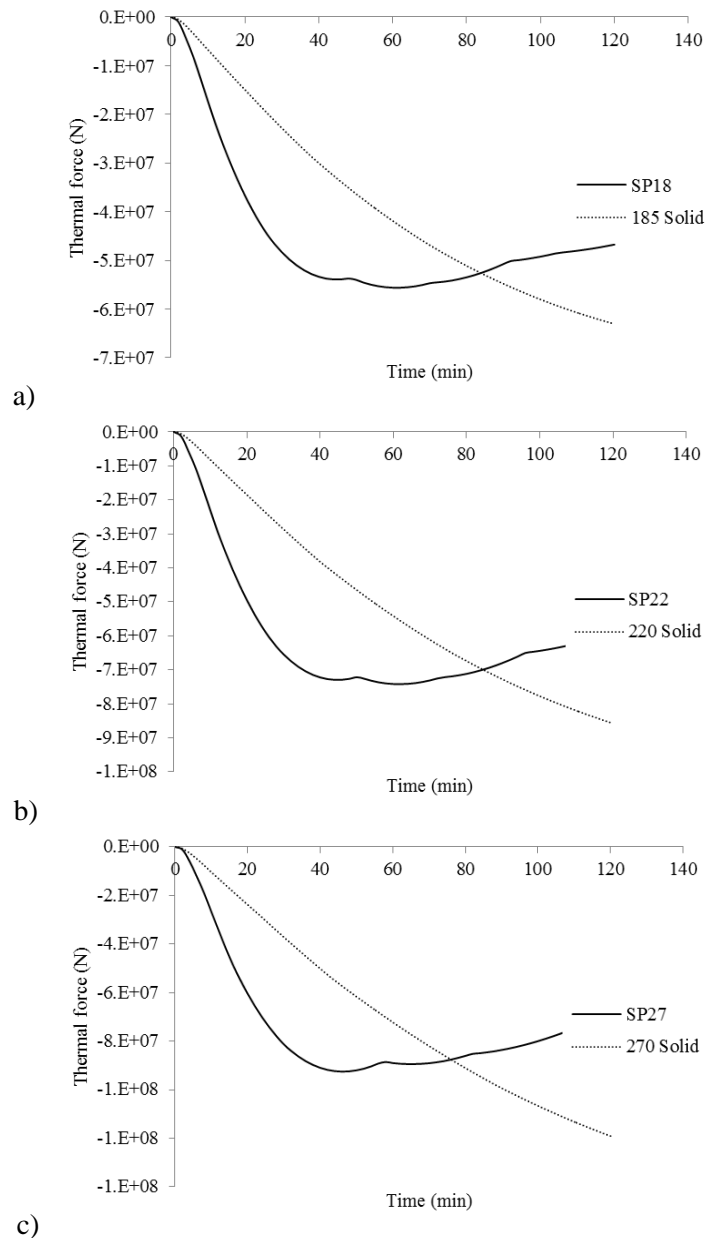


**Figure 3.7 – thermal force, as defined in equation 3.6, in a) the SP 18 hollow core slab and a 185 mm deep concrete slab b) the SP 22 hollow core slab and a 220 mm deep concrete slab and c) the SP 27 hollow core slab and a 270 mm deep concrete slab**

### 3.5 Calculation of temperature dependent prestressing force

The prestressing force applied by the tendons will change as the tendons heat up, both as a result of thermal expansion of the tendons, the reduction in stiffness of the tendons and the thermal expansion of the surrounding concrete. Assuming no loss of bond between tendon and concrete, this change in prestressing force may in a simplified way be estimated as:

$$F_{pre,T} = E_{pre,T} \frac{F_{pre,\infty} \alpha_c \Delta T_c}{E_{pre,\infty} \alpha_s \Delta T_s} \quad (3.8)$$

Note that this is conceptually different from the stress in the tendons which is reported in the finite element modelling results, since the numerical modelling also includes in the tendon stress the effects of deflection of the cross section under both load and thermal deflections which are not accounted for here. This additional stress in the tendons due to deflection of the loaded section will be accounted for when determining the overall capacity of the section later. Regarding the coefficient of thermal expansion and the ratio of thermal strain in the concrete and thermal strain in the steel; for simplicity it may be assumed that the coefficient of thermal expansion of steel and concrete are the same and so this term is neglected in the calculations which follow.

The bar diameter and prestressing load in the three hollow core slabs which are being used to exemplify the methodology are summarised in Table 3.1. In the DIFT test report, the SP 27 slabs had two types of reinforcement, of different diameters and different level of prestress. The smaller diameter bar is used to study the section here.

**Figure 3.1 - bar diameter and prestressing load in the hollow core slabs**

<b>Slab designation</b>	<b>Bar diameter</b>	<b>Prestressing load</b>
SP 18	9.3 mm	58kN
SP 22	9.3 mm	58 kN
SP 27	12.5 mm	104 kN

The temperature dependent prestressing forces in the three hollow core slabs described in the previous section are shown in Figure 3.8 a. Figure 3.8 b shows the temperature dependent prestressing force in the monolithic concrete slabs. The cover to the prestressing tendons in the monolithic slabs is the same as the cover to the tendons in the hollow cores, 25 mm. Note that this is only based on the increase in temperature of the tendon; and that if deflections were added to this there would in fact be an increase in the prestressing force early on in the fire exposure. This is a result of the deflection of the cross section under heating. A detailed discussion of the timeline of tendon response in prestressed concrete slabs is given in [48].

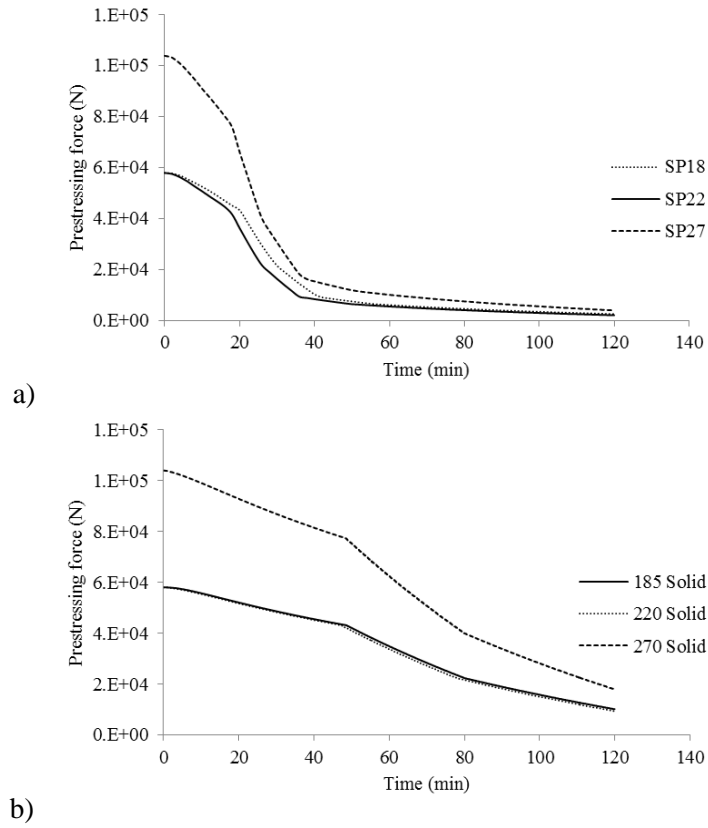


**Figure 3.8 Temperature dependent prestressing load in a) hollow core slabs, and b) monolithic slabs of varying thickness**

The effect of the hollow cores, effectively slowing the conduction from the bottom flange to the top flange in the hollow core slabs, is evident in the change in prestressing load with temperature. The hollow core slabs have a higher temperature in the lower flange than the same area of the monolithic concrete slab, meaning that the tendons become hotter faster in the hollow core slabs, losing their prestress at a greater rate.

### 3.6 Calculation of thermally induced displacements

This temperature dependent prestressing force acts in the opposite direction to the curvature caused by the thermal gradient in the section. As with the thermal gradient, this prestressing force acts on the modified section at an eccentricity to the centroid determined by the modified centroid of the section and the initial eccentricity of the prestressing tendons. The resultant moment in the section is given by equation 3.9. This causes curvature of the slab, which is of the opposite sign to the thermal moment, and which reduces the equivalent contraction strain. Reduction of the prestressing force reduces this tendon induced curvature.

$$M_{pre,T} = F_{pre,T}(y_c - y_{pre}) \quad (3.9)$$

The total moment in the section, obtained from superposition of the thermal moment and the moment from prestressing, is:

$$M_{tot} = M_T + M_{pre,T} \quad (3.10)$$

The curvature caused by the prestressing moment is given by:

$$\phi_{pre,T} = M_{pre,T} / (E_c I_m) \quad (3.11)$$

And the total curvature of the section is the sum of the thermal curvature and the curvature caused by the prestressing moment:

$$\phi_{tot,T} = \phi_{pre,T} - \phi_T \quad (3.12)$$

The total end rotations of the slab are given by:

$$\omega_{tot} = L \phi_{tot,T} / 2 \quad (3.13)$$

And the equivalent contraction strain at the ends of the slab as a result of the total curvature can be approximated by:

$$\varepsilon_{tot} = 1 - \sin(\omega_{tot}) / \omega_{tot} \quad (3.14)$$

Multiplying this by the length gives the translation at the end of a simply supported slab under thermal loading.

$$u = L \varepsilon_{tot} \quad (3.15)$$

Cameron [44] proposed a cubic equation which describes the thermally deflected shape of a 1-dimensional element which is subject to a thermal gradient and a thermal force, equation (3.16a). Substituting the thermal moment and the thermal force in this equation for the total moment and the total force in the section, equations 3.9 and the sum of 3.8 and 3.1, provides the equation for the deflected shape of a prestressed concrete element under thermal loading, accounting for the effect of temperature on the prestressing tendon:

$$w_T^3 + \left( \frac{4I_m}{A_m} - \frac{4F_T L^2}{\pi^2 E_c A_m} \right) w_T + \frac{16M_T L^2}{\pi^3 E_c A_m} \quad (3.16a)$$

$$w_{pre,T}^3 + \left( \frac{4I_m}{A_m} - \frac{4F_{tot} L^2}{\pi^2 E_c A_m} \right) w_{pre,T} + \frac{16M_{tot} L^2}{\pi^3 E_c A_m} \quad (3.16b)$$

To exemplify the calculation of vertical displacement at the mid span and lateral displacement at the supports, the same cross sections as described above are studied, assuming a length of 6.57 metres. This was the length of some of the slabs in the Hong Kong Vantaa fire described in chapter 1.1.3.

Figures 3.9 and 3.10 show the vertical displacement and the lateral displacement respectively for the different section sizes. As would be expected the hollow core slabs have a larger displacement at the midspan and at the ends under heating than the monolithic concrete slabs. However, the evolution of this displacement over time reflects also the shape of the thermal moment and thermal force evolution, shown in Figures 3.6 and 3.7 above. In terms of design of prestressed concrete construction, the lateral displacement in particular is of interest as it provides an indication of the minimum

bearing width which would be required of the supporting construction, assuming that thermal deflection dominates over load induced deflection up until failure.

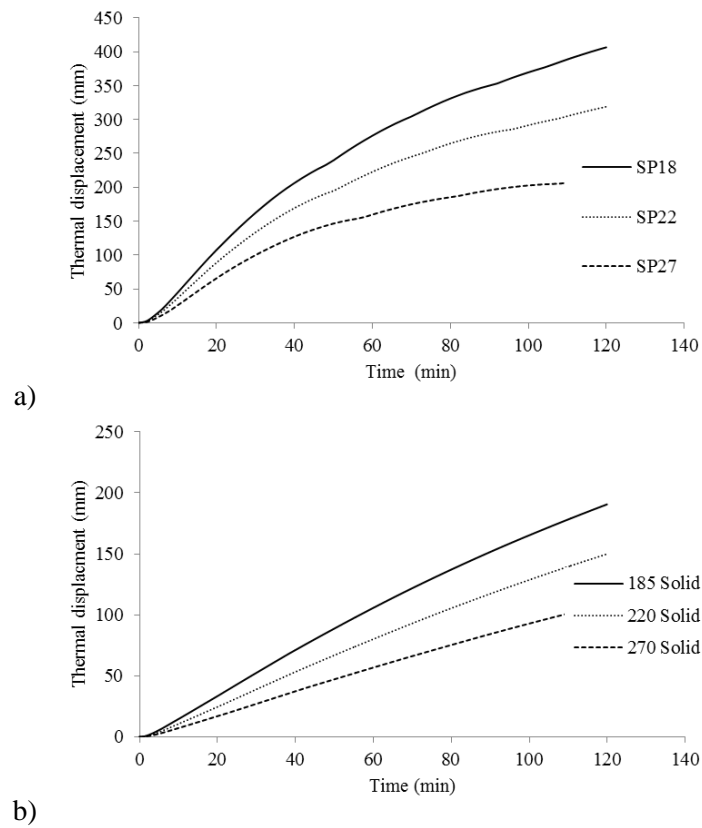


**Figure 3.9 Midspan displacement under standard fire exposure of a) hollow core slabs, and b) monolithic slabs of varying thickness**

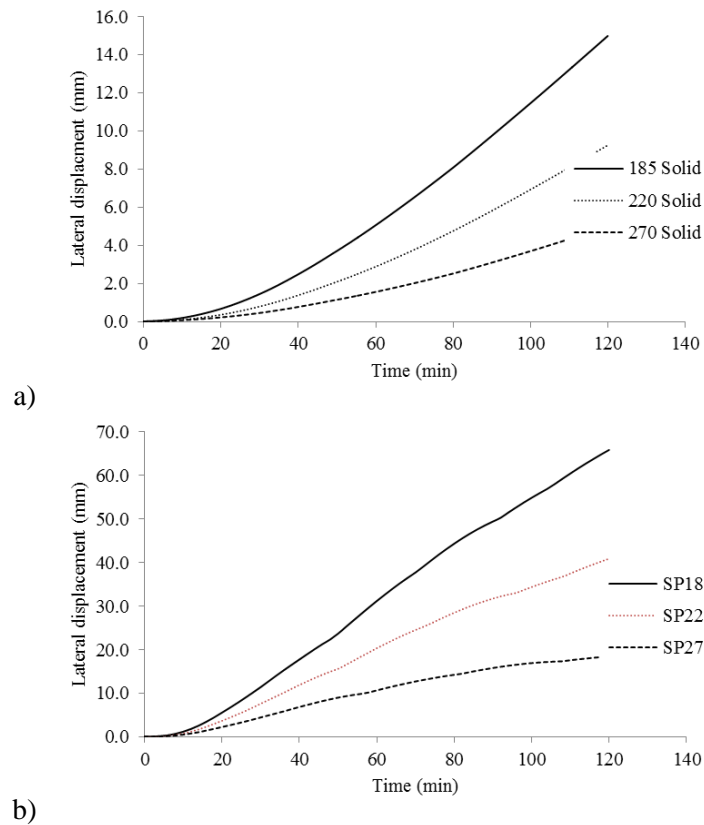


**Figure 3.10 Lateral displacement at the supports of simply supported a) hollow core slabs, and b) monolithic slabs of varying thickness under standard fire exposure**

### 3.7 Load bearing capacity

Consider an arbitrary prestressed concrete cross section, Figure 3.11 a). The depth to the reinforcement is denoted  $d$ , width of the section is  $b$ , and depth to the neutral axis is  $x$ . The initial distribution of strain in the concrete under application of only the prestressing load is indicated by the dashed line in Figure 3.11 b) and has magnitude  $\epsilon_c$  at the level of the prestressing steel. With application of an external moment up until failure of the section, the distribution of strain changes and the compressive strain in the upper surface of the concrete increases until the ultimate strain,  $\epsilon_{cu}$ . Correspondingly the compressive strain at the level of reinforcement is reduced and a tensile strain develops at the level of the tendon. Now considering the effect of temperature, an additional strain is also added to the concrete which corresponds with the thermal expansion strain through the depth of the section, denoted  $\epsilon_T$  in Figure 3.11 b).

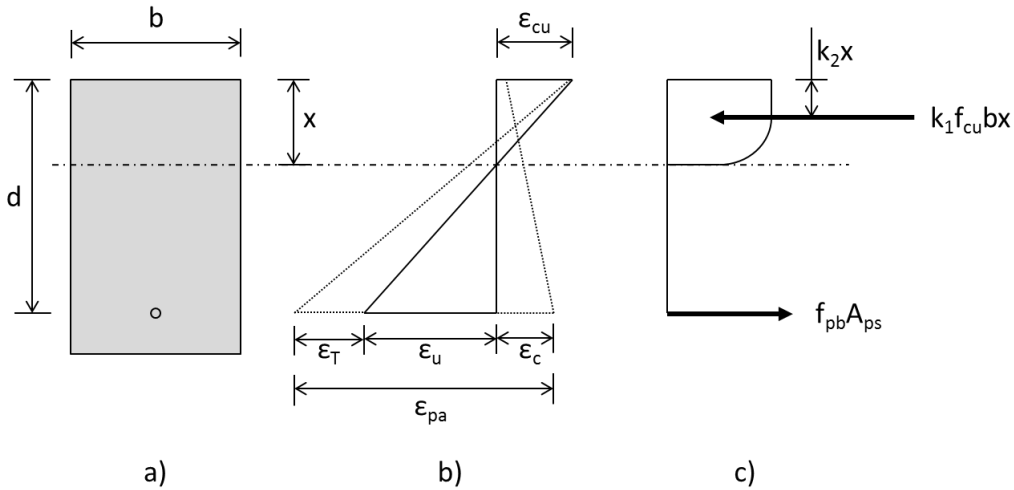


**Figure 3.11 – a) geometry, b) distribution of strains in concrete, and c) forces on a prestressed concrete section.**

If the tendon strain at the ultimate state is denoted  $\epsilon_{pb}$ , this is equal to the sum of the concrete strain at the ultimate state at this depth, as well as the strain resulting from the prestressing force in the steel:

$$\epsilon_{pb,T} = \epsilon_{pre,T} + \epsilon_{pa} \quad (3.17)$$

The strain in the prestressing steel,  $\epsilon_{pre,T}$  can be determined from the temperature dependent prestressing force as:

$$\epsilon_{pre,T} = \frac{F_{pre,T}}{A_{ps} E_{pre,T}} \quad (3.18)$$

The change in the strain in the concrete at the level of the prestressing steel from the initial compressive strain to the tensile strain when the ultimate external moment is applied,  $\epsilon_{pa}$ , is given by, including the term for the thermal expansion strain:

$$\epsilon_{pa} = \epsilon_c + \epsilon_u + \epsilon_T \quad (3.19)$$

This is the additional strain which the prestressing steel has to accommodate in order for the concrete at the upper surface of the section to reach its ultimate strain. Recognising that:

$$\epsilon_u = \epsilon_{cu} \frac{d - x}{x} \quad (3.20)$$

Substituting equations 3.20 and 3.19 into 3.17 and rearranging gives the following expression for the neutral axis depth,  $x$ :

$$x = \frac{\epsilon_{cu} d}{\epsilon_{pb,T} + \epsilon_{cu} - \epsilon_{pre,T} - \epsilon_c - \epsilon_T} \quad (3.21)$$

The tension-compression couple shown in Figure 3.11 c) is provided by the tensile force in the prestressing tendon, acting at the depth of the tendons and the compressive force in the concrete area under compression, acting at a depth given by the geometric centroid of

the stress block. This introduces the coefficients  $k_1$  and  $k_2$  which describe the characteristic shape of the concrete stress block, and which may be obtained from literature (commonly  $k_1=0.45$  and  $k_2=0.405$ ). The compressive force,  $F_{cc}$ , is given by:

$$F_{cc} = k_1 f_{cu} b x \quad (3.22)$$

Where  $f_{cu}$  is the compressive yield strength of the concrete. The tensile force,  $F_{ts}$ , is given by:

$$F_{ts} = A_{ps} \sigma_{pb} \quad (3.23)$$

Where  $A_{ps}$  is the area of the prestressing steel, and  $\sigma_{pb}$  is the stress in the reinforcement, Substituting equations 3.22 and 3.23 into equation 3.21 and rearranging yields the following expression for the stress in the steel at the ultimate moment of the section.

$$\sigma_{pb} = \frac{k_1 f_{cu} b}{A_{ps}} \frac{\varepsilon_{cu} d}{\varepsilon_{pb,T} + \varepsilon_{cu} - \varepsilon_{pre,T} - \varepsilon_c - \varepsilon_T} \quad (3.24)$$

This could either be solved along with the stress strain curve diagram of the prestressing tendon, or if it can be assumed that the tendon is behaving elastically, then the following substitution can be made:

$$\sigma_{pb} = \frac{k_1 f_{cu} b}{A_{ps}} \frac{\varepsilon_{cu} d}{\sigma_{pb} / E_{pre,T} + \varepsilon_{cu} - \varepsilon_{pre,T} - \varepsilon_c - \varepsilon_T} \quad (3.25)$$

Upon rearrangement this yields a quadratic which may be solved for  $f_{pb}$ :

$$\frac{1}{E_{pre,T}} \sigma_{pb}^2 + (\varepsilon_{cu} - \varepsilon_{pre,T} - \varepsilon_c - \varepsilon_T) \sigma_{pb} - \frac{k_1 f_{cu} b \varepsilon_{cu} d}{A_{ps}} = 0 \quad (3.26)$$

Once  $\sigma_{pb}$  is known then equation 3.22 and 3.23 can be used to determine the depth of the concrete stress block and then moments can be taken about the centroid to determine the ultimate moment of the section. In the case of hollow core slabs with the depth of the concrete stress block below the depth of the upper flange, then the above equations need to be modified to reflect the reduced thickness of the section with the depth. It should also be noted that the breadth in equations (3.22), (3.24), (3.25) and (3.26) should be based on the effective area of the heated cross section, as given in equation (3.4), with the depth set equal to the actual depth to the prestressing tendons of the section.

Using the crushing strain from the Eurocode, of  $\varepsilon_{cu}=0.0025$ , and a concrete compressive strength of 40 MPa, the evolution of the ultimate moment of the hollow core and monolithic concrete sections described above is shown in Figures 3.12a) to c). To aid comparison these results have been normalised against the ambient capacity of the sections. These follow much the same trend as the evolution of the prestressing load on the tendons, Figure 3.8, with a gradual reduction in the ultimate moment in the monolithic prestressed concrete slabs over the course of 2 hours of fire exposure; whereas the hollow core prestressed slabs have a steeper initial reduction in ultimate moment as a result of the hotter concrete in the region of the prestressing tendons.

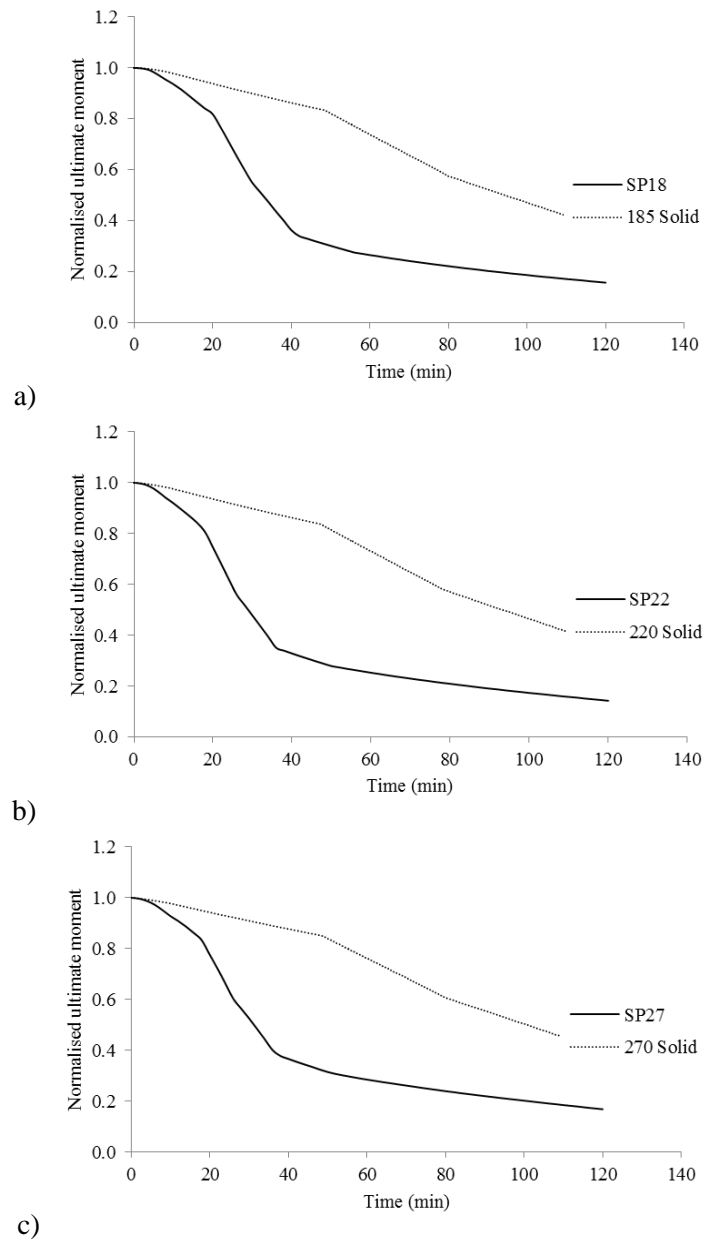


**Figure 3.12 – normalised ultimate moment in a) the SP 18 hollow core slab and a 185 mm deep concrete slab b) the SP 22 hollow core slab and a 220 mm deep concrete slab and c) the SP 27 hollow core slab and a 270 mm deep concrete slab**

## 4 Influencing the ultimate moment of prestressed concrete construction

In this section the influence of 3 parameters on the overall behaviour of prestressed concrete construction in fire are discussed: the distance of the prestressing tendons from the exposed surface of the concrete; the initial prestressing level; and the overall geometry of the prestressed section.

All of the studies are undertaken using the analytical method described in the previous chapter.

### 4.1 Cover to reinforcement

In order to evaluate the effects of the depth of cover to the prestressing tendon in prestressed concrete sections, the sections described in the previous section were subject to further analysis, changing the cover to the tendon from 12 mm to 40 mm in the case of the hollow core sections and the 185 mm deep monolithic concrete section; and from 12 to 50 mm and 12 to 90 mm in the 220 mm deep and 270 mm deep monolithic concrete sections respectively. Some changes to the material properties were also made for this study, the concrete stiffness was assumed to be 36 000 MPa and the compressive strength was assumed to be 60 MPa. The crushing strain was also assumed to be 0.0035.

The ultimate moment in the hollow core sections SP 18, SP 22, and SP 27 are shown in Figures 4.1 a) to c) respectively. These are all shown normalised against their original capacity. Throughout all of the examples which are shown, it can be seen that a hollow core section with a greater cover to the tendons loses less of its initial capacity in comparison with a hollow core section with lower cover to the tendons. This however is offset against the initial ultimate moment of the section as a result of a reduced lever arm with increased cover to the tendon since the cross section is maintained the same.

Similarly, the ultimate moment in the monolithic prestressed concrete sections of depth 185 mm, 220 mm, and 270 mm is shown in Figure 4.2. Again, these are normalised against their ambient capacity. As with the hollow core sections, these monolithic prestressed concrete sections benefit from an increased cover to the reinforcement in terms of the residual capacity after increasing periods of fire resistance, although it is not as significant as for the hollow core slabs.

The overall behaviour of the hollow core and monolithic concrete sections and their dependence on the cover to the tendons is shown in Figure 4.3 a) and b) respectively. The dashed line indicates the largest cover to the tendon and the dash-dot line indicates the smallest cover to the tendon.

For hollow core slabs, the smallest tendon cover provides the highest ultimate moment at ambient and for short periods of fire exposure, however a larger tendon cover, while it provides a lower ultimate moment at ambient does provide a higher ultimate moment after a prolonged period of fire exposure in comparison with a smaller cover to the tendon. The effect of the higher temperatures occurring relatively early in the prestressing tendon in the hollow core slabs means that the benefit in terms of increased ultimate moment of the cross section is actually lost during fire exposure of the hollow core slabs. There is a transition at which the benefit in a higher lever arm to the tendons is offset by the increased heating of the tendon closer to the surface. The time at which this occurs

obviously varies, but in the examples which were studied this occurred at just after half an hour of standard fire exposure.

In the case of the monolithic slabs, in the examples which were studied, there is no point at which a larger lever arm stops being beneficial compared with a larger cover to the tendon.

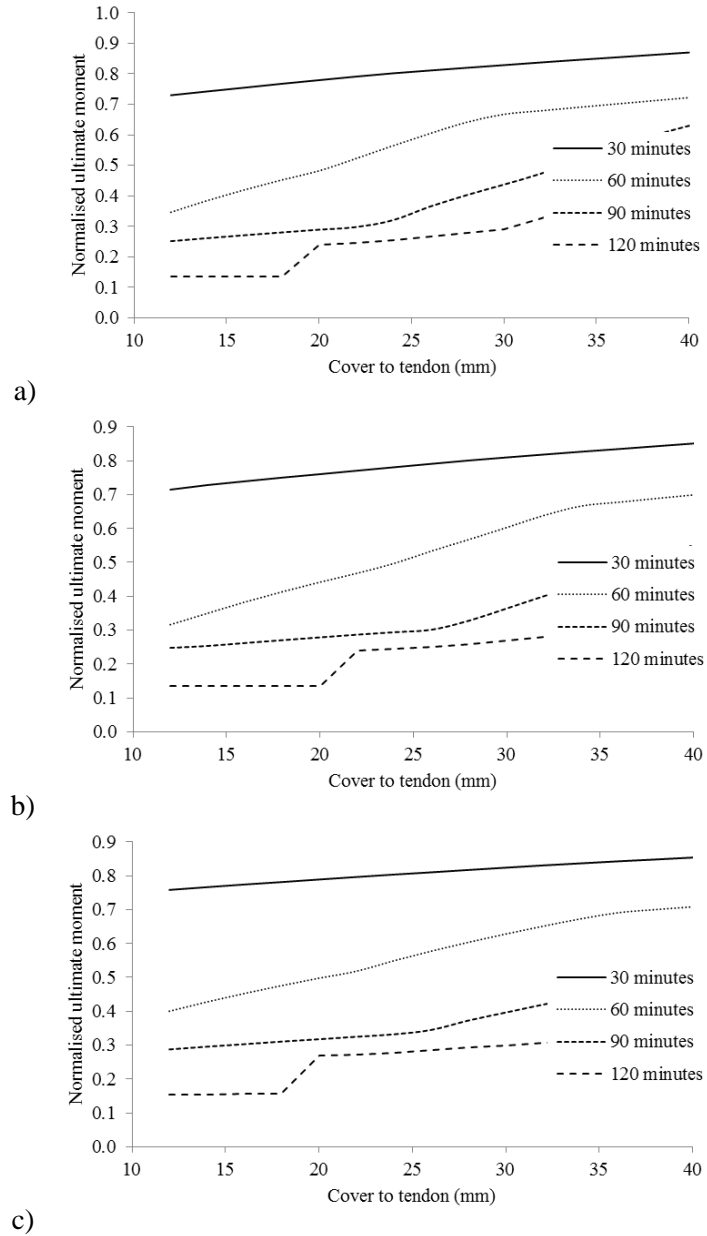


**Figure 4.1 – normalised ultimate moment of hollow core sections at different times of exposure to a standard fire, plotted against the cover to the tendon: a) an SP 18 section; b) an SP 22 section; and c) an SP 27 section**

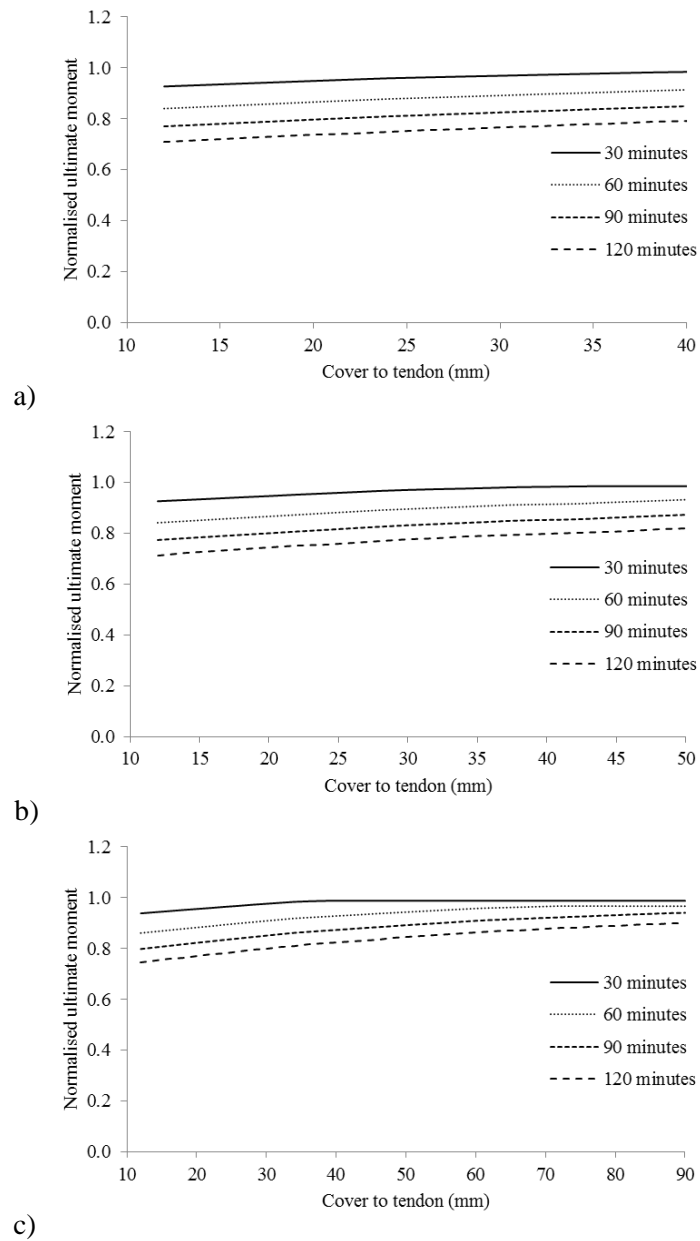


**Figure 4.2 – normalised ultimate moment of monolithic prestressed concrete sections at different times of exposure to a standard fire, plotted against the cover to the tendon: a) a 185 mm deep section; b) a 220 mm deep section; and c) a 270 mm deep section**

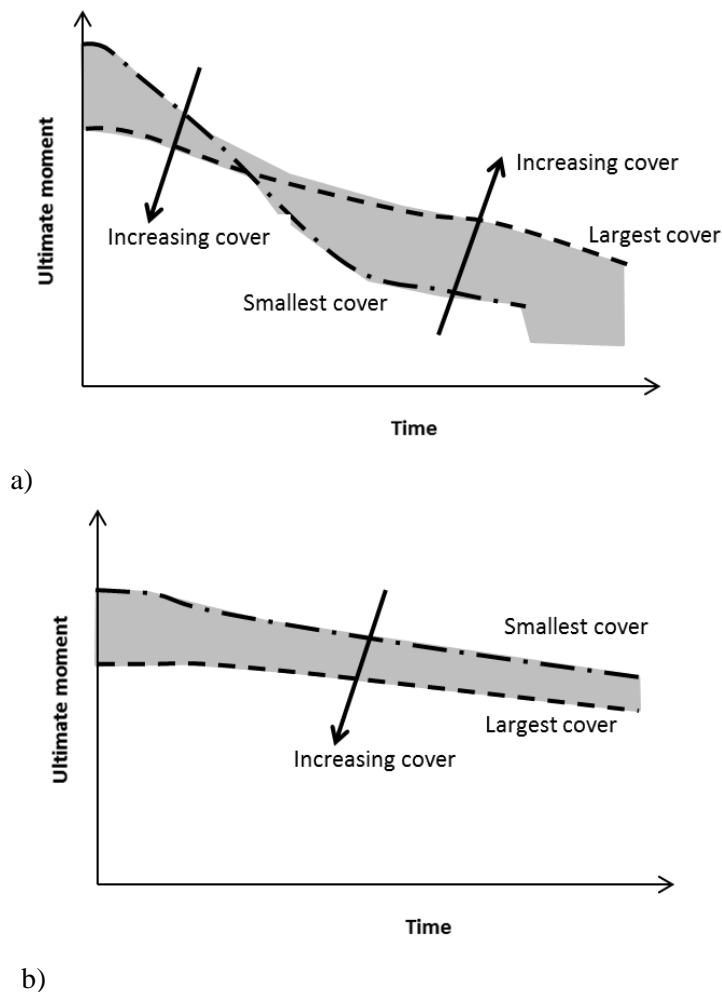


**Figure 4.3 – schematic showing the effect of increasing cover to the prestressing tendon on the short and the long term ultimate moment of a) a hollow core section, and b) a monolithic concrete section exposed to fire**

## 4.2 Prestressing force

To evaluate the effect of the prestressing force on the long term evolution of the ultimate moment of a prestressed hollow core and monolithic sections, the same concrete sections as described in the previous section of this report are studied, subject to the same changes as were made when evaluating the impact of the cover to the prestressing tendons.

In each of the sections, the prestressing force was varied from 40 % to 120 % of the prestressing load which was used to demonstrate the analytical method.

The normalised ultimate moment of the hollow core sections is shown in Figure 4.4 and the normalised ultimate moment of the monolithic sections is shown in Figure 4.5. In all cases the ultimate moment of the section at different times of fire exposure is plotted against the initial prestressing force in the section. As opposed to the depth to the prestressing tendons the initial prestress has limited impact on the evolution of the ultimate moment during fire exposure of either the hollow core or the monolithic concrete prestressed sections.

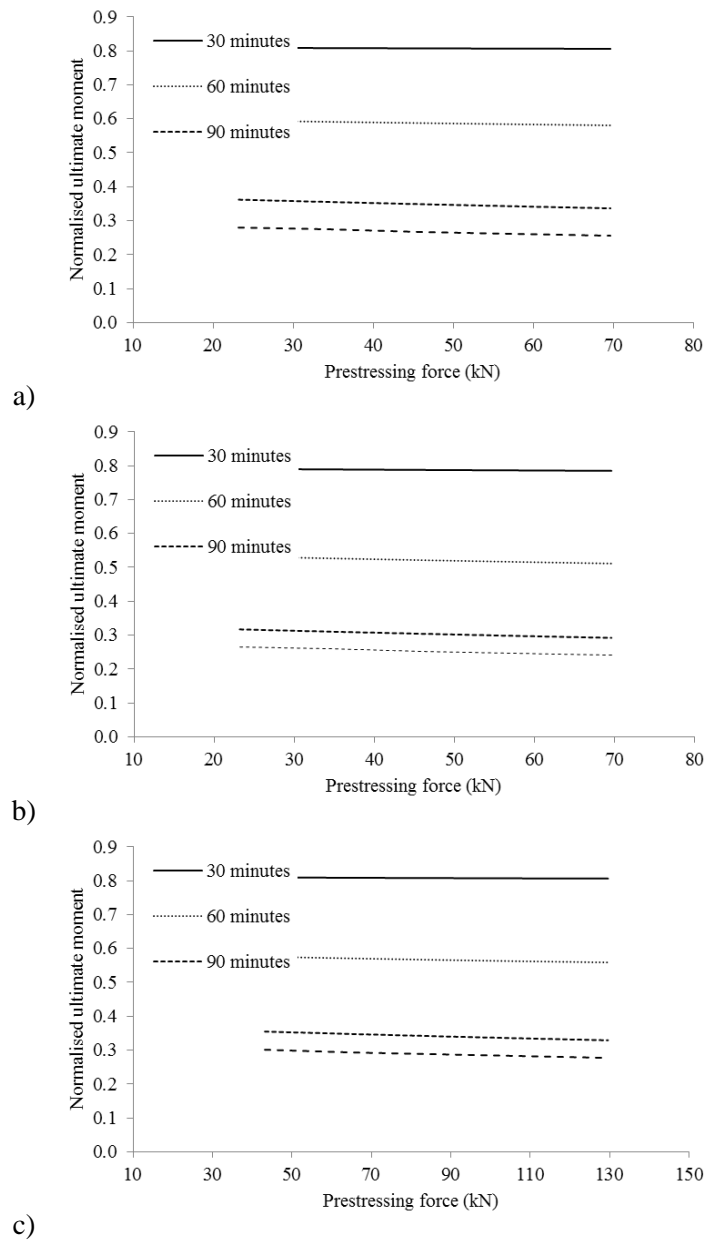


**Figure 4.4 – normalised ultimate moment of hollow core sections at different times of exposure to a standard fire, plotted against the prestressing force of the tendon: a) an SP 18 section; b) an SP 22 section; and c) an SP 27 section**

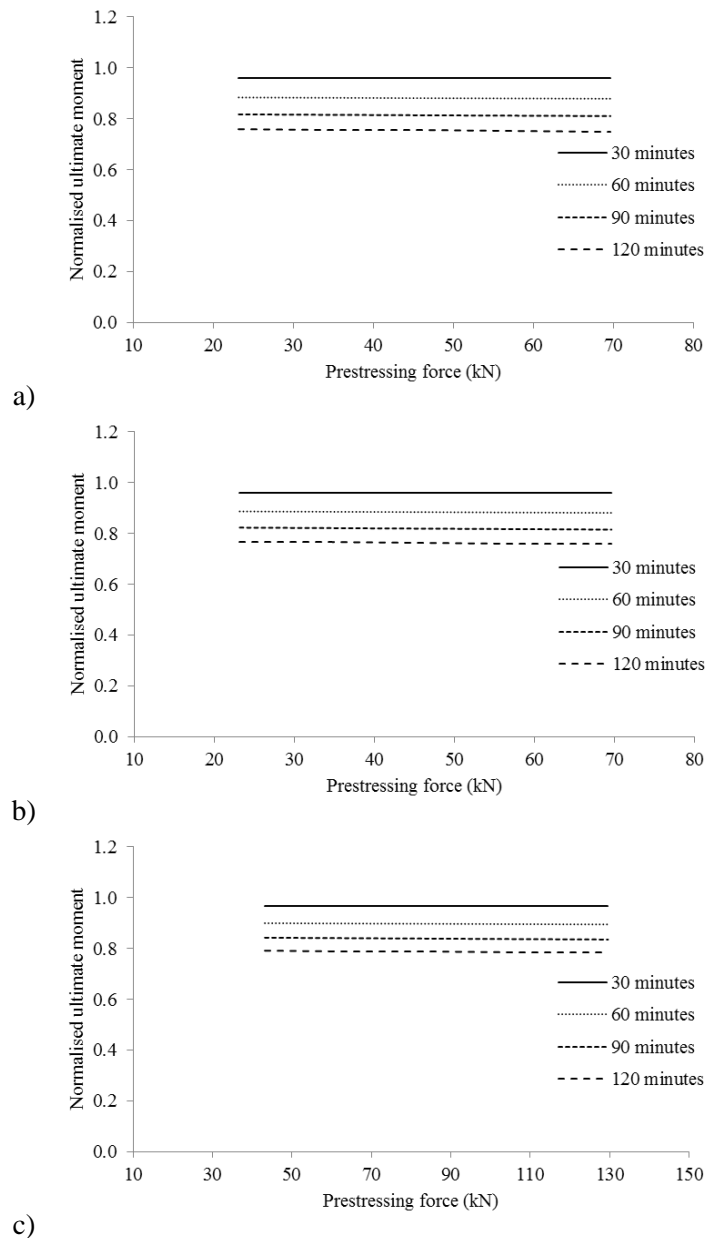


**Figure 4.5 – normalised ultimate moment of monolithic prestressed concrete sections at different times of exposure to a standard fire, plotted against the prestressing force of the tendon: a) a 185 mm deep section; b) a 220 mm deep section; and c) a 270 mm deep section**

### 4.3 Section geometry

The single biggest influence on the evolution of the ultimate moment of resistance of prestressed hollow core floors exposed to fire seems to be the increased temperature of the lower flange and the correspondingly higher temperatures of the prestressing tendons in comparison with monolithic concrete floors.

As discussed previously, this higher temperature of the lower flange is a result of the resistive effect of the voids in transferring heat from the lower flange through the web and into the upper flange. Therefore any design feature which alleviates this effect and slows the rate of increase of heat of the prestressing tendons will have a positive influence on the ultimate moment of hollow core floors under fire exposure.

The following changes to the geometry of the cross section would have such an effect:

1. Increasing the depth of the lower flange, which will increase the volume available for storage of thermal energy, thus reducing the temperatures of the lower flange.
2. Decreasing the diameter of the hollow cores / increasing the width of the web / increasing the spacing between the hollow cores, this will reduce the resistive effect of the reduction in in-plane area for heat transfer through the section, thus reducing the temperature of the lower flange.

It is however noted that any changes which could be made to the geometry of hollow core sections to improve the fire resistance would have a knock on effect on the ambient load bearing capacity of the hollow core sections.

With regards to the monolithic concrete sections, the effect of increasing the cover to the tendon or of increasing the prestressing force has minimal impact on the overall response of the section as it is heated.

## 5 Discussion and conclusions

The intention of this study was to identify contributing factors which may help to understand the behaviour of hollow core and prestressed concrete construction exposed to fire. The project was prepared in response to the fire which occurred in Vantaa in Finland in 2010, where hollow core slabs exposed to fire performed poorer than may be expected based on their fire resistance rating. That is not to say that any construction which has been certified as fire resistant for 2 hours when exposed to a standard fire should be expected to last for 2 hours when exposed to any fire, however the failure time of just over an hour suggests that further work is needed to understand the response of hollow core slabs exposed to fire.

A wealth of numerical analyses has been undertaken in the literature, in response to the car park fire in Rotterdam in the Netherlands in particular. This has of course contributed significantly to understanding the response of hollow core slab construction and modelling and detailing of the transfer region in particular. Nevertheless, other work which is referenced in this report suggests that the concrete material model used for analyses could have a significant effect on the predicted response of prestressed concrete construction exposed to fire and so additional work was undertaken in this project to apply an alternative concrete material model to numerical analyses of hollow core slab sections.

The numerical analyses which was carried out confirmed the impact of different material models, and showed that an explicit consideration of transient strain in concrete material models seems to result in a better correlation to experimental results, and globally the behaviour is as expected in terms of, e.g. crack formation. However, the availability of good quality test data from fire tests of hollow core slabs for validation of models is limited in the open literature and so the application of these models to studying various parameters affecting the response of hollow core units exposed to fire is difficult to justify.

In order to study different parameters of interest, therefore, an analytical method was proposed which is based on the design of prestressed concrete construction at ambient, but which accounts for the response of the heated prestressing tendon as well as the effect of heating on the concrete cross section. The resulting method is applicable to both hollow core and prestressed concrete construction and allows for a comparison of the effects of heating on these two types of construction. Based on these analyses, it may be concluded that:

1. Curvature resulting in midspan and lateral displacements in hollow core slabs could be used to estimate the bearing width needed from supporting construction.
2. Hollow core concrete construction experiences a far higher thermal gradient and resulting thermal moment than monolithic concrete construction. This is a result of the geometry of the cross section which effectively traps heat in the lower flange.
3. The trapping of heat in hollow core construction leads to a faster loss of prestressing force on the cross section compared with a monolithic section. This contributes to a faster reduction in the ultimate moment of hollow core slabs compared with monolithic concrete construction with the same concrete cover.

The analytical method was used to carry out a simple parametric study of prestressed hollow core and monolithic concrete construction. Two parameters were varied, the depth to the prestressing tendon (cover to the tendon) and the initial prestressing force.

4. It was found that the initial prestressing force has little effect on the evolution of the ultimate moment of the cross section under fire exposure.
  
5. However changing the prestressing tendon depth had a significant effect on the evolution of the ultimate moment under fire exposure. A shallow tendon with little cover has higher capacity at ambient and under fire exposure for a short duration, whereas a tendon with a large amount of cover has a lower ambient capacity, but retains more of this capacity for longer under fire exposure.

Considering the geometry of hollow core slabs and points 3 and 5 above, it is possible that small changes in the geometry and the tendon placement could result in a better retention of ultimate moment capacity in the event of fire.

Finally, however, the difficulty in validation of the methods used in this report must be noted. Further work is needed in this regard by means of a well-controlled and well instrumented test of a hollow core slab in fire.

## 6 References

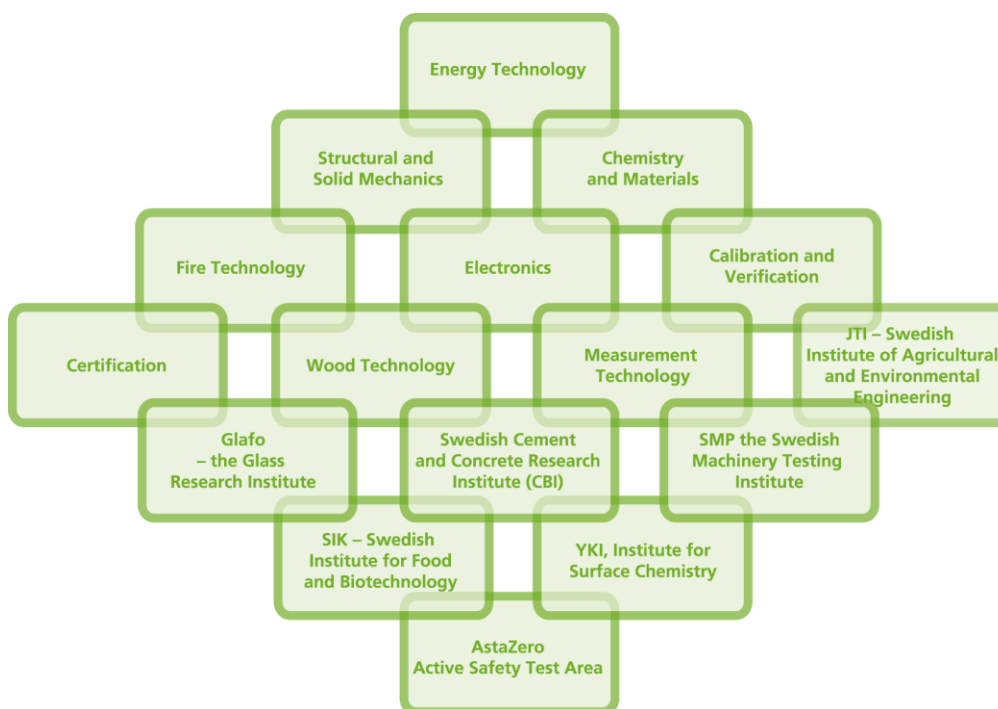
- [1] Janze W. et al “Structural behaviour of prestressed concrete hollow core floors exposed to fire” BIBM report published January 24, 2014, 226 pages
- [2] Anderberg Y., Thelandersson S. “Stress and deformation characteristics of concrete at high temperatures 2. Experimental investigation and material behaviour model” Bulletin 54, Lund Institute of Technology, Lund, Sweden , 1976
- [3] Anderberg Y. “Fire-exposed hyperstatic concrete structures – An Experimental and theoretical study” Bulletin 55, Lund Institute of Technology, Lund, Sweden , 1976
- [4] O. Petterson, “Practical need of scientific material models for structural fire design-- General review,” Fire safety journal, vol. 13, pp. 1 - 8, 1988.
- [5] Y. Anderberg and O. Petterson, Brandteknisk dimensionering av betong konstruktioner. Stockholm: Statens råd för byggnadsforskning, 1991.
- [6] Investigation of Broadgate Phase 8 Fire. SCI, 1991.
- [7] T. Z. Harmathy and T. T. Lie, “Fire Test Standard in the Light of Fire Research,” in ASTM STP 464, 1970, pp. 85 - 97.
- [8] M. O’Connor, “Behaviour of a multi-storey steel framed building subjected to fire attack,” Journal of Constructional Steel Research, vol. 46, no. 1-3, p. 295, Jun. 1998.
- [9] C. Bailey, “The tensile membrane action of unrestrained composite slabs simulated under fire conditions,” Engineering Structures, vol. 22, no. 12, pp. 1583-1595, Dec. 2000.
- [10] A. Usmani, N. Cameron, “Limit capacity of laterally restrained reinforced concrete floor slabs in fire,” Cement and Concrete Composites, vol. 26, no. 2, pp. 127-140, Feb. 2004.
- [11] C. G. Bailey, “Efficient arrangement of reinforcement for membrane behaviour of composite floor slabs in fire conditions,” Journal of Constructional Steel Research, vol. 59, pp. 931-949, 2003.
- [12] K. G. Bernander and P. Ab, “Studium av orsaken till tidigt ras,” Design, no. September, 1996.
- [13] P. G. Gambarova, R. Felicetti, A. Meda, and P. Rive, “Proceedings of the Workshop Fire Design of Concrete Structures : What now ? What next ?,” in Civil Engineering, 2004.
- [14] F. Ruiz, A. Muttoni, and J. Kunz, “Strengthening of Flat Slabs Against Punching Shear Using Post-Installed Shear Reinforcement,” Aci Structural Journal, no. 107, 2011.
- [15] Y. Mirzaei, “Post-Punching Behavior of Reinforced Concrete Slabs,” École polytechnique fédérale de Lausanne, 2010.
- [16] A. H. K. M. Smith; B. T. Stratford; L. Bisby; Punching shear of reinforced concrete slabs under fire conditions: experiment vs. design; The First International Conference on Structural Safety under Fire & Blast CONFAB 2015 2nd-4th September 2015; Glasgow – United Kingdom
- [17] R.K.S. Al Hamd; M. Gillie.; Y. Wang; M.M. Rasheed; Punching shear – eccentric load and fire conditions; The First International Conference on Structural Safety under Fire & Blast CONFAB 2015 2nd-4th September 2015; Glasgow – United Kingdom
- [18] C. Kleinman and J. Linssen, “Brand en kanaalplaat- vloeren,” Cement, vol. 5, pp. 4-5, 2011, in Dutch

- [19] I. Pielkenrood, "brief 8 juni met bijlage 16 06 2011." BFBN Betonproducten, 2011; in Dutch
- [20] de Feiter, M.P.; Breunese, A.J.; Onderzoek brand parkeergarage Lloydstraat, Rotterdam; Efectis Netherlands report number: 2007 – Efectis – R0894
- [21] "Hong Kong variety shop burns down in Vantaa," Helsinki Times, 27-Dec-2010.
- [22] "Hong Kong Vantaa Razed," YLE.fi, 24-Dec-2010.
- [23] K. Lehtinun and T. Rasmus, Tavaratalon sortumiseen johtanut tulipalo Vantaalla (in Finnish). 2011.
- [24] www.svenskbetong.se, (12-04-23)
- [25] A. L. Materazzi, M. Brecolotti, "Fire behaviour of HPLWC hollow core slabs: full scale furnace tests and numerical modelling", Workshop on: Fire design of concrete structures: What now? What next?, fib Task Group 4.3, Milan, Italy, Dec. 2 - 4, 2004
- [26] J. J. Chang, "Computer Simulation of Hollowcore Concrete Flooring Systems Exposed to Fire", Doctoral thesis, Department of Civil Engineering, University of Canterbury Christchurch, New Zealand, 2007
- [27] Fellingner, J.; Shear and anchorage behaviour of fire exposed hollow core slabs; Heron 50(2005), issue 4
- [28] J. Gales, L.A. Bisby, M. Gillie; Unbonded Post Tensioned Concrete Slabs in Fire- Part I- Experimental Response of Unbonded Tendons under Transient Localized Heating. Journal of Structural Fire Engineering. 2 (2011) 139-153
- [29] J. Gales, L.A. Bisby, M. Gillie; Unbonded Post Tensioned Concrete Slabs in Fire - Part II – Modelling Tendon Response and the Consequences of Localized Heating. Journal of Structural Fire Engineering. 2 (2011) 155-171.
- [30] J.H.H. Fellingner, "Shear and Anchorage Behaviour of Fire Exposed Hollow Core Slabs" Doctoral thesis, TU Delft, ISBN 90-407-2482-2, 2004
- [31] www.eota.be, ETAG 23 and 24, (16-03-21)
- [32] EN 1992-1-2:2004 Design of concrete structures, Part 1-2: General rules - Structural fire design
- [33] A. V. Acker, "Research versus Industry", Workshop on: Fire design of concrete structures: What now? What next?, fib Task Group 4.3, Milan, Italy, Dec. 2 - 4, 2004
- [34] Schneider, U.; Horvath, J.; Behaviour of ordinary concrete at high temperatures; Research reports of Vienna University of Technology, Institute of Building Materials, Building Physics and Fire Protection Vol. 9, Vienna, 2003.
- [35] Law, A.; The assessment and response of concrete structures subject to fire; PhD thesis; The University of Edinburgh 2010
- [36] Khoury, G.; Fire and concrete: from materials behaviour to application; International workshop on fire design of concrete structures from materials modelling to structural performance; University of Coimbra; November 2007
- [37] Anderberg, Y.; The impact of various material models on structural fire behaviour prediction; Structures in fire '08; Singapore 2008
- [38] Gernay, T.; Franssen J.-M.; A formulation of the Eurocode 2 concrete model at elevated temperature that includes an explicit term for transient creep; Fire Safety Journal 51 (2012) 1 – 9
- [39] Gernay, T.; Effect of transient creep strain model on the behaviour of concrete columns subjected to heating and cooling; Fire technology 48 (2012) 313 – 329

- [40] Huang, S.; Burgess, I.; Huang, Z. and Plank, R.; Effect of transient thermal strain on the buckling-of slender concrete and concrete-filled columns in fire; Structures in fire '08; Singapore 2008
- [41] D. Lange, R. Jansson, A comparison of an explicit and an implicit transient strain formulation for concrete in fire, 11th Symposium of the International Association for Fire Safety Science; Christchurch, 2014
- [42] Andersen, N.E.; Lauridsen, D.H.; Technical report X52650 Part 2: Hollow core concrete slabs, Basismiddel projekt X52650; Danish institute of fire technology, April 1999
- [43] Comite Euro-International du Beton; CIB-FIP Model code 1990: Design code; 1993
- [44] A.S. Usmani, , J.M. Rotter, S. Lamont, A.M. Sanad, M. Gillie; Fundamental principles of structural behaviour under thermal effects; Fire Safety Journal Volume 36, Issue 8, November 2001, Pages 721–744; (DOI:10.1016/S0379-7112(01)00037-6)
- [45] A. S. Usmani and S. Lamont; Key events in the structural response of a composite steel frame structure in fire; Fire and Materials 2004; 28:281–297 (DOI: 10.1002/fam.856)
- [46] N.J.K Cameron; The behaviour and design of composite floor systems in fire. The University of Edinburgh, 2003
- [47] D. Lange; J. Sjöström, Mechanical response of a partially restrained column exposed to localised fires, Fire Safety Journal, 2014, DOI: 10.1016/j.firesaf.2014.05.013
- [48] J. Sjöström, D. Lange, R. Jansson, L-Boström; Anisotropic curvature and damage of post-tensioned concrete slabs during fire testing; submitted to Fire Technology

## SP Technical Research Institute of Sweden

Our work is concentrated on innovation and the development of value-adding technology. Using Sweden's most extensive and advanced resources for technical evaluation, measurement technology, research and development, we make an important contribution to the competitiveness and sustainable development of industry. Research is carried out in close conjunction with universities and institutes of technology, to the benefit of a customer base of about 10000 organisations, ranging from start-up companies developing new technologies or new ideas to international groups.



## SP Technical Research Institute of Sweden

Box 857, SE-501 15 BORÅS, SWEDEN

Telephone: +46 10 516 50 00, Telefax: +46 33 13 55 02

E-mail: [info@sp.se](mailto:info@sp.se), Internet: [www.sp.se](http://www.sp.se)

[www.sp.se](http://www.sp.se)

Fire Technology

SP Report 2014:52

ISBN 978-91-88349-54-5

ISSN 0284-5172

More information about publications published by SP: [www.sp.se/publ](http://www.sp.se/publ)



SP Technical Research Institute of Sweden  
Box 857,  
SE-501 15 BORÅS, SWEDEN  
Telephone: +46 10 516 50 00,  
Telefax: +46 33 13 55 02  
Email: [info@sp.se](mailto:info@sp.se), Internet: [www.sp.se](http://www.sp.se)  
[www.sp.se](http://www.sp.se)

OUR SPONSORS & PARTNERS:



## RAPPORTER UTGIVNA AV BRANDFORSK 2016:

- 2016:1** Utrymning i långa trappor uppåt:  
Utmattning, gånghastighet  
och beteende
- 2016:2** Förflyttning vid utrymning
- 2016:3** Dubbelglasfasader  
- En brandteknisk förstudie
- 2016:4** Utveckling och validering av  
enkla och praktiska modeller för  
beräkning av brandgastemperaturer  
i rum/brandceller
- 2016:5** Brandskyddsfärgens funktion vid  
riktiga bränder
- 2016:6** Detaljutformning av moderna  
betongkonstruktioner för att  
förbättra brandmotståndet
- 2016:7** ETANKFIRE - Släckning av en  
etanolcistern för att förbättra brand  
motståndet
- 2016:8** Metoder för att följa upp  
efterlevnad av brandskyddskrav



**1979 bildades Brandforsk som svar på behovet av ett gemensamt organ för att initiera och finansiera forskning och utveckling inom brandsäkerhetsområdet.**

Brandforsk är statens, försäkringsbranschens och industrins gemensamma organ för att initiera, bekosta och följa upp olika slag av brandforskning.

Huvudman för Brandforsk är Brandskyddsföreningen och verksamheten leds av en styrelse och bedrivs i form av projekt vid universitet och högskolor, forskningsinstitut, myndigheter och företag.



**Brandforsk**

Årstaängsvägen 21 c  
Box 472 44, 100 74 Stockholm  
Tel: 08-588 474 14  
[brandforsk@brandskyddsforeningen.se](mailto:brandforsk@brandskyddsforeningen.se)